The Search for the X (1750) in Ultra Peripheral Collisions at STAR

BY

NILANTHI WARNASOORIYA

A THESIS

Submitted to the Faculty of the Graduate School of

Creighton University in partial fulfillment of

the requirements for the degree of Master of Science

in the Department of Physics

Omaha, NE (August, 2003)

CHAPTER 1

THE RELATIVISTIC HEAVY ION COLLIDER (RHIC)

The Relativistic Heavy Ion Collider (RHIC) is a large research facility at Brookhaven National Laboratory (BNL) on Long Island, New York. RHIC is the first collider in the world that is capable of colliding heavy ions at very high energies. Heavy ions are nuclei of large atoms such as gold with more or fewer electrons than usual or no electrons at all. RHIC uses primarily ions of gold which have had their entire outer cloud of electrons removed. RHIC features two identical concentric rings, “blue” and “yellow”, circulating in opposite directions with a circumference of 2.4 miles. In these rings, gold ions are accelerated to a very high energy in opposite directions. In the first RHIC run in the year 2000, gold nuclei were accelerated to a center of mass energy of 130 GeV/nucleon. In 2001, the energy was 200 GeV/nucleon. RHIC can also accelerate other species such as protons, carbon, sulphur, copper, deuterium etc. In the year 2003 RHIC run, gold-gold, gold-deuterium and proton-proton collisions were studied.

The ion beams are not continuous, they consist of bunches of 1.1×10^{9} ions. Collisions occur at regular intervals when a bunch from one beam crosses the bunch of the other beam. The time between two crossings is 112ns and crossings occur at a rate of 8.9 MHz. In the 2001 RHIC run, there were 60 bunches per ring with a peak luminosity of 5×10^{26} $cm^{-2}s^{-1}$. This was 2.5 times greater than the design average luminosity.[1] The luminosity is the number of gold ions in the beam per area per time. It is an important factor since the production rate for a particle of interest is given as product of the luminosity of the collider and the cross section for the reaction.

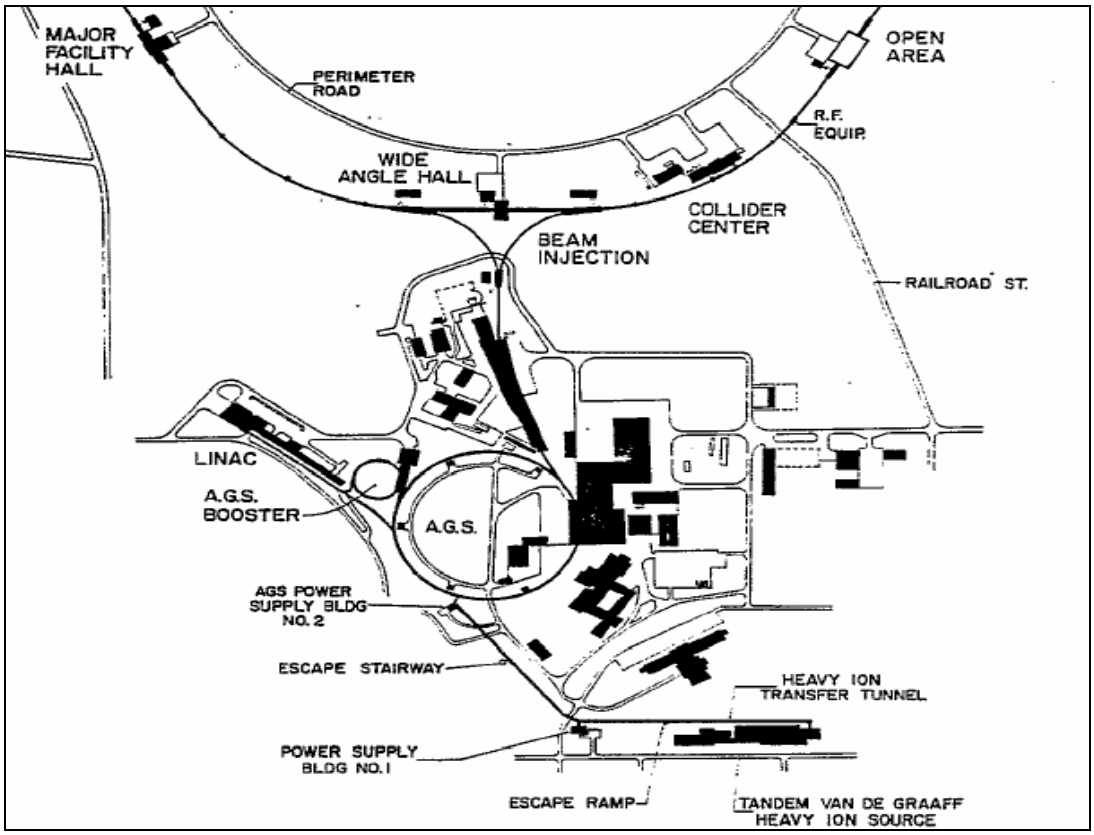

Figure (1.1): Main features of the RHIC ring. Gold atoms are ionized at the Tandem Van de Graff heavy ion source at the bottom right hand side of the figure and then sent to the RHIC ring via the heavy ion transfer line and the AGS.[2]

Gold atoms are ionized at the Tandem Van de Graaff accelerator as shown in Figure (1.1). These ions are then accelerated and sent to the heavy ion transfer tunnel. The heavy ion transfer line sends these ions to the AGS (Alternating Gradient Synchroton) Booster. The booster is a circular accelerator that provides the ions more energy. As a result, in the booster, the ions gain higher speeds and get closer to the speed of light (~37% the speed of light). Then these ions are sent to the AGS, where they get more energy and finally reach a velocity of 99.7% the speed of light. These ions are then directed to the RHIC ring in opposite directions, one “blue” and one “yellow”, where the two ion beams are steered to collide at six different locations as shown in Figure (1.2).

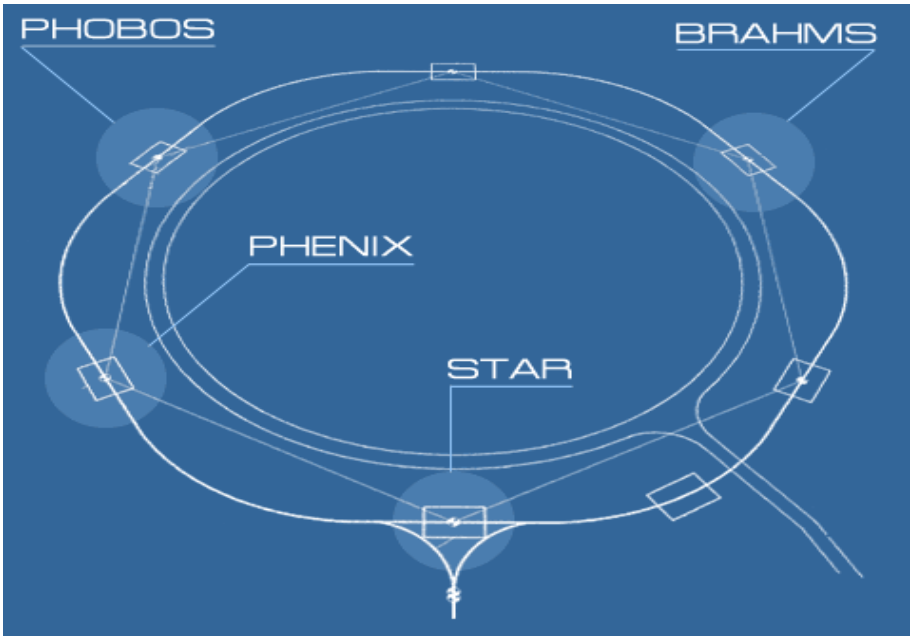

Figure (1.2): The six intersection points of the RHIC ring are shown as white dots inside rectangles. There are four experiments at the ring including the STAR detector, which is located at the injection point.[3]

Four experiments, PHOBOS, PHENIX, BRAHMS and STAR are located at four of the intersection points of the RHIC ring. Their locations are shown in Figure (1.2).

CHAPTER 2

THE SOLENOIDAL TRACKER AT RHIC (STAR)

STAR (the Solenoidal Tracker At RHIC) is one of the four large experiments at RHIC. At the time the data for this thesis was collected, the STAR detector included a large solenoidal magnet, a central trigger barrel, a time projection chamber, a forward time projection chamber, a silicon vertex tracker and two zero degree calorimeters. The detector is shown in Figure (2.1). The solenoidal magnet provides a uniform magnetic field parallel to the beam line, with a design strength of 0.5T. The total magnet length is 6.9m. Small correction coils are used to improve the field uniformity. The purpose of the trigger barrel is to select interesting signals and to reject background events. The time projection chamber (TPC) reconstructs the paths of charged particles to identify particles and their characteristics. The silicon vertex tracker (SVT), with a length of 42cm, is used to locate primary and secondary vertices. The zero degree calorimeters are used to detect neutrons.

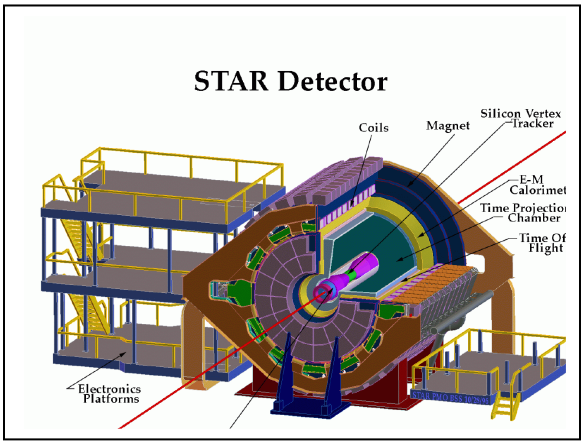

Figure (2.1a): The STAR detector.[3]

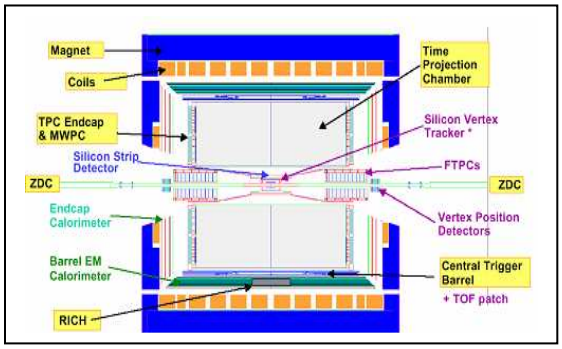

Figure (2.1b): Side view of the STAR detector. The figure shows the main parts of the detector. The two gold beams come from both sides and collide at the center of the TPC.[3]

The most important parts of the STAR detector for this study are the time projection chamber (TPC), the zero degree calorimeter (ZDC) and the central trigger barrel (CTB). These are described in greater detail in sections (2.1) to (2.3).

(2.1) The Time Projection Chamber (TPC)

The TPC, which can be considered the 'heart' of STAR, is a massive device with a length of 4.2 meters and a width of 4.2 meters. It is located inside a uniform magnetic field with a design strength of 0.5T. The TPC consists of inner and outer field cages with radii of 0.5m and 2.1m respectively and a high voltage membrane at the center, as shown in Figure (2.2). An electric field parallel to the beam line is caused by the potential difference between the center membrane and the end-caps. The field points from the center membrane toward each of the end-caps.

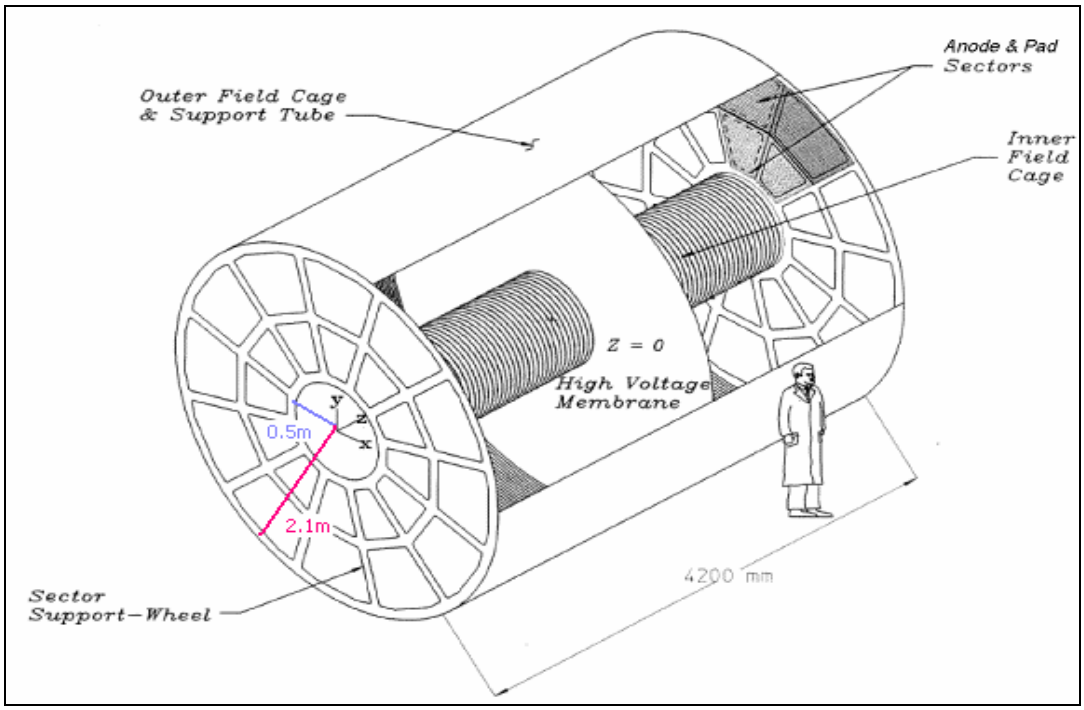

Figure (2.2): STAR time projection chamber. The voltage difference between the center membrane and the end-caps creates an electric field parallel to the beam line.[4]

Charged particles emerging from the interaction region at the center of the barrel ionize gas molecules. Due to the electric field (130V/cm) created by the membrane, these ionized gas particles drift in the longitudinal direction toward the end-caps as shown in Figure (2.3). On the way to end-caps, these ionized gas particles collide with other gas particles. If there were no such collisions, the ions would drift with a constant acceleration. Due to the collisions, they can instead be modeled as drifting with a constant (average) velocity. This drift velocity is 5.5cm/μs for the TPC.

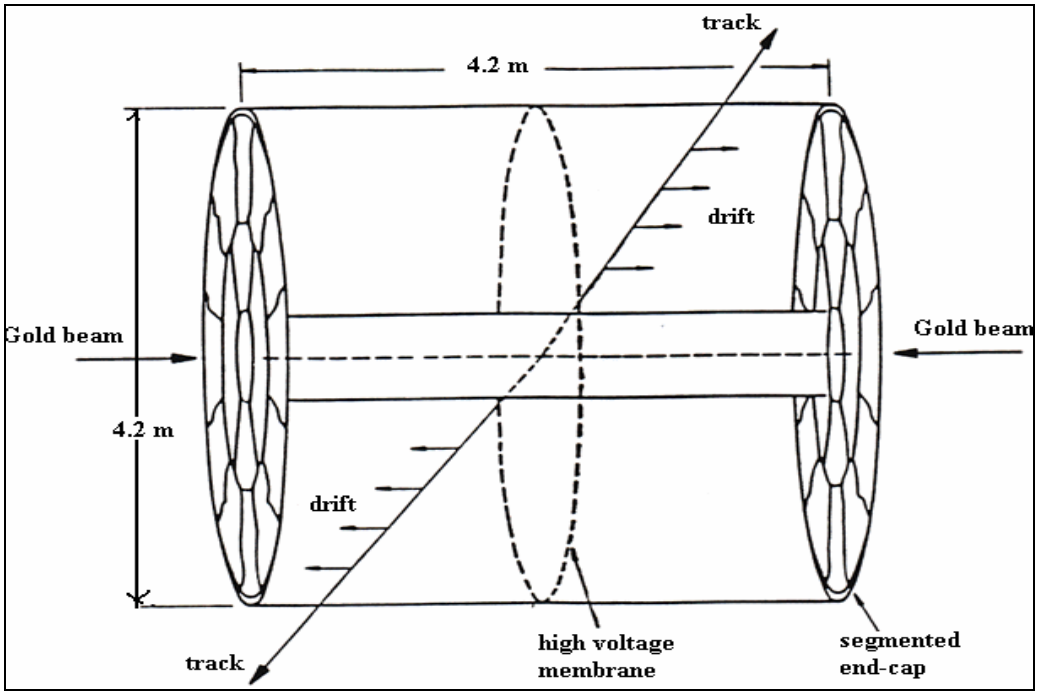

Figure (2.3): Charged particles emerging from the interaction region ionize gas molecules. In this figure these are shown as tracks. Due to the electric field, these ionized gas particles drift in the longitudinal direction toward the end-caps where detection occurs.

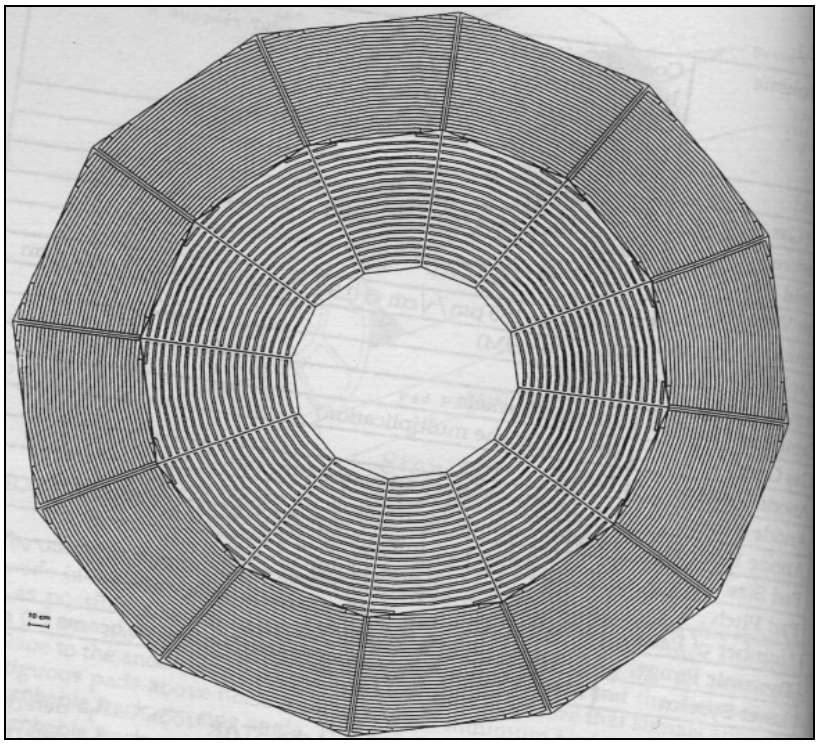

Figure (2.4): The TPC end cap. There are 12 sectors, each of which is divided into two parts. Both outer and inner sectors are arranged in circular rows with smaller pads in the inner sector.[4]

The trails of ionized gas can be detected at the end-caps. A detailed drawing of the end-cap is shown in Figure (2.4). Each end cap has 12 sectors which are divided into two parts, the inner and the outer. Both inner and outer sectors have circular rows of pads. Pads provide the spatial location of the track. For each track, the drift time provides the coordinate parallel to the beam line and the induced signals on the pad rows provide the two coordinates perpendicular to the beam line. With these three coordinates, the tracks of particles produced in collisions are reconstructed.

(2.2) The Zero Degree Calorimeter (ZDC)

There are calorimeters located on each side of the detector, ±18 meters from the interaction point. Since they are close to the beam line and detect particles that travel at approximately zero degree angles (~2 mrad), these are called zero degree calorimeters. Nuclear fragments that are remnants of the collisions continue down the beam pipe. These fragments can decay by single and multiple neutron emissions, producing neutrons with very small transverse momenta (i.e., component of the momentum perpendicular to the beam line). The neutrons travel almost parallel to the beam pipe and can be detected by the ZDCs. Before the particles reach the ZDCs, they go through a dipole magnet, which is located at about 10m from the interaction point. Due to the field of the magnet, charged particles are deflected and do not enter the ZDCs.

When neutrons strike the ZDCs, they cause an electric signal proportional to their total energy. Analog to digital converters convert these signals to digital signals. These digital signals are analyzed to determine the number of neutrons emitted. This helps to determine the impact parameter of the collision. With ultra peripheral collisions, where nuclei physically miss each other, there are very few neutrons in the ZDCs. When nuclei partially overlap, some fragments can travel down the beam pipe. These fragments decay by neutron emission, and we can see many neutrons in the ZDCs. With very central collisions there are no intact fragments traveling down the beam pipe, and therefore we see fewer neutrons in the ZDCs. In the case of ultra peripheral collisions, the ZDC signals can be used to identify whether the outgoing nuclei are in excited states.

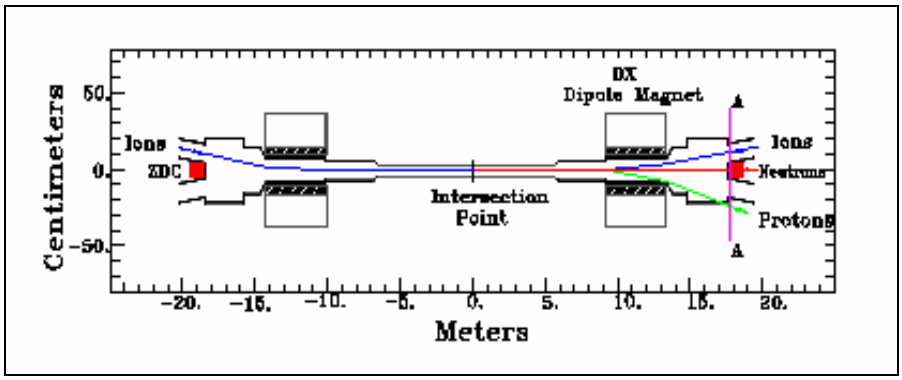

Figure (2.5): View of the ZDC location. Two dipole magnets are located at 10m from the interaction point. Charged particles are deflected due to the field of the magnet. Neutrons, which do not deflect, are detected by the ZDCs.[5]

(2.3) The Central Trigger Barrel (CTB)

The main task of the central trigger barrel (CTB) is fast detection of charged particles. The CTB can be used as a fast trigger since it is capable of processing and transmitting signals at close to the speed of light. It is used to select interesting signals and to reject background events. Compared to the CTB, the TPC is a slow detector since it has to wait for the tracks to drift to the end caps.

The trigger barrel consists of a cylinder of 120 trays, each containing two scintillator slats as shown in Figure (2.6). The trays are located around the outside of the TPC in a barrel of radius 2m and length 4m. Each scintillator has one photomultiplier tube (PMT). A PMT is an electronic photon detector based on the photoelectric effect. When a photon of sufficient energy is incident on the photo cathode of the PMT, a single electron is ejected. This single photoelectron is accelerated through a potential difference in the first stage of the PMT. The accelerated electron then hits a secondary electrode, ejecting other electrons by its electromagnetic interaction. These secondary electrons are accelerated and hit a second electrode and the process is repeated causing a multiplication

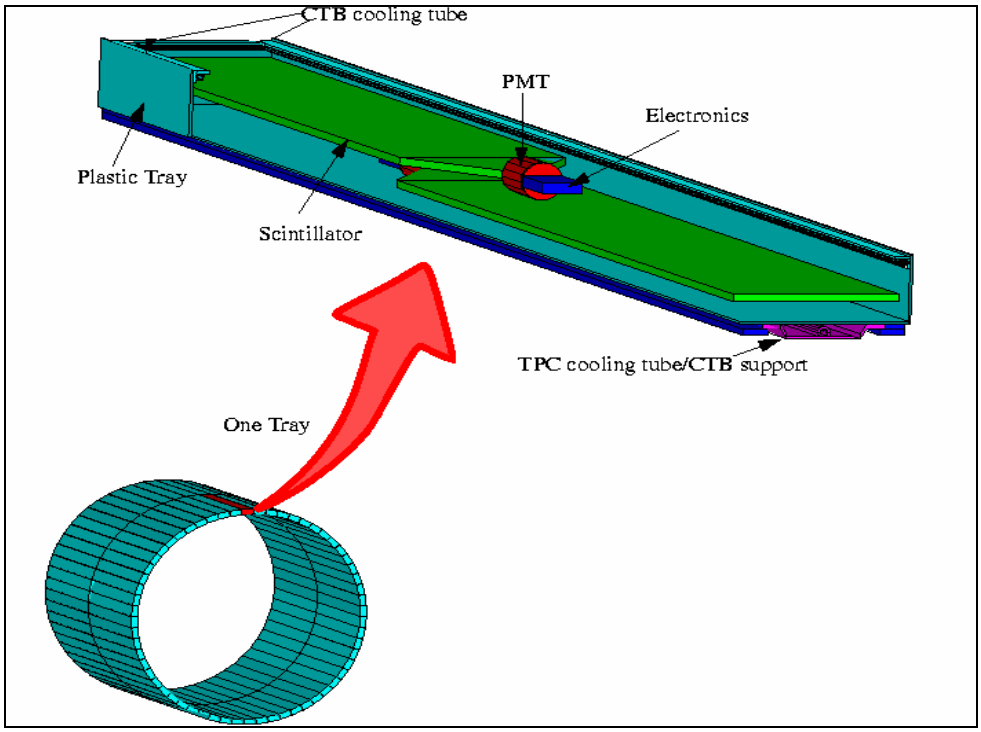

Figure (2.6): The Central Trigger Barrel. It consists of a cylinder of 120 trays, each containing two scintillator slats.[6]

of electrons. These electrons produce an electric signal which can be detected by an electrical circuit. The output signal of the PMT is proportional to the number of particles that pass through the scintillator. When the signal is greater than a certain threshold we say the slat was hit. The threshold signal can be controlled according to our needs. A certain number of slats must be hit before triggering occurs. The number of slats also can be controlled. When a sufficient signal is present in the CTB, the event is recorded. The criteria for recording an event can be varied to fit the kind of physics we want to study. For example, in ultra peripheral collisions, very few tracks are produced. A trigger for this type of events will require few slats to be hit.

CHAPTER 3

ULTRA PERIPHERAL COLLISIONS

The primary goal of STAR is to study the early stage of the universe by creating a quark-gluon plasma (QGP) in the laboratory. A QGP is a state where quarks can be found as neither baryons (bound state of 3 quarks) nor mesons (bound quark-anti quark pairs), but as a plasma of unbound quarks and gluons. (i.e. QGP is a state where isolated quarks can exist.) It is believed that until 10 microseconds after the Big Bang (origin of the universe), such a state existed. Physicists at STAR try to create such a state by colliding heavy ions at very high energies. To study the QGP, physicists need central collisions, but there are other types of collisions that also have very interesting physics. Three types of collisions are being studied at STAR: central collisions, peripheral collisions and ultra peripheral collisions. In central collisions one nucleus overlaps completely with the other. The collisions where nuclei overlap partially are known as peripheral collisions and the collisions where nuclei physically miss each other are known as ultra peripheral collisions. Central collisions are used to study signatures of a possible quark-gluon plasma. However many other interesting physics topics can be studied with ultra peripheral collisions.

STAR studies ultra peripheral interactions at very high energies. These collisions are considerably different from central collisions since in ultra peripheral collisions the ions can remain in their ground state. The multiplicity of these events is low (i.e., few charged particles are produced), compared to the thousands of particles produced in central collisions. Thus ultra peripheral collisions are easier to track since, in general,

there are less than 10 tracks per event, but harder to trigger since there are thousands of background events to be removed.

(3.1) Ultra peripheral collisions:

Ultra peripheral collisions are defined as electromagnetic or strong interactions where the nuclei physically miss each other. For these collisions, the impact parameter, b, should be larger than twice the radius of the nucleus as shown in Figure (3.1). There are three types of interactions, photon-photon interactions, photonuclear interactions and Pomeron-Pomeron interactions. When each nucleus emits a photon, the interaction is known as a photon-photon interaction and when only one nucleus emits a photon, the interaction is known as a photonuclear interaction. When nuclei interact via the strong nuclear force, the exchange particles are Pomerons and these interactions are known as Pomeron-Pomeron interactions. These three types of interaction are described briefly in sections(3.2) to (3.4). This study will focus on the photonuclear interactions.

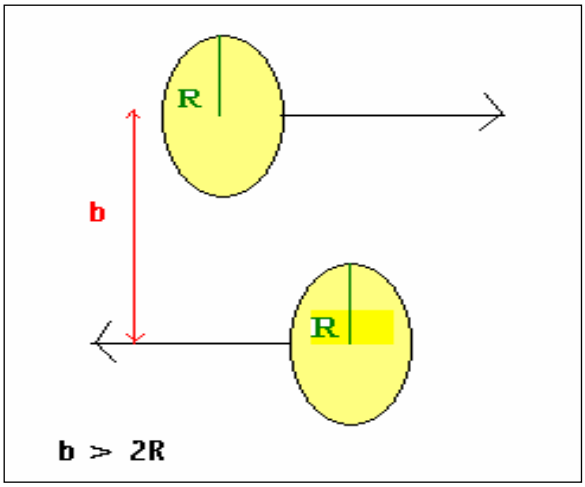

Figure (3.1): The impact parameter of ultra peripheral collisions. In ultra peripheral collisions the impact parameter, b, is larger than twice the radius of the nucleus.

(3.2) Photon-Photon Interactions:

Photon-photon interactions occur when the two nuclei interact by electromagnetic fields, each nucleus emitting a photon. The charge of photons is zero. Therefore, in order to conserve charge, the total charge of the final products should be zero. Because photons have spin 1, the total spin of two photons can be 0, 1 or 2. Therefore, the resultant particles should have total spin 0, 1 or 2. The baryon number and the lepton number for photons is zero. This can be conserved by producing baryon-anti baryon or lepton-anti lepton pairs as they have opposite baryon or lepton numbers. The resultant particles from photon-photon interactions are either meson-anti meson pairs or lepton-anti lepton pairs with total spin 0, 1 or 2.

(3.3) Photonuclear Interactions:

In photonuclear interactions, a photon emitted by one gold nucleus fluctuates into a quark-anti quark pair as shown in Figure (3.2). When the second nucleus interacts with the wave function of the photon, this quark-anti quark pair may emerge as a neutral vector meson. Neutral vector mesons can be ρ, ω, ϕ or J/Ψ mesons. Since photons have zero charge and spin one, the resultant meson also has zero charge and spin one. (i.e., neutral vector meson). These neutral mesons cannot be detected directly for two reasons. First, they are neutral and therefore do not leave tracks in the TPC and, second, they have very short lifetimes. The neutral vector mesons decay into charged particles which can be observed. We focused on photonuclear interactions because these interactions have high rates of occurring. Some physics topics that are studied in the Ultra Peripheral Collisions

Program in STAR are meson pair production, ρ meson production and the search for more exotic mesons.

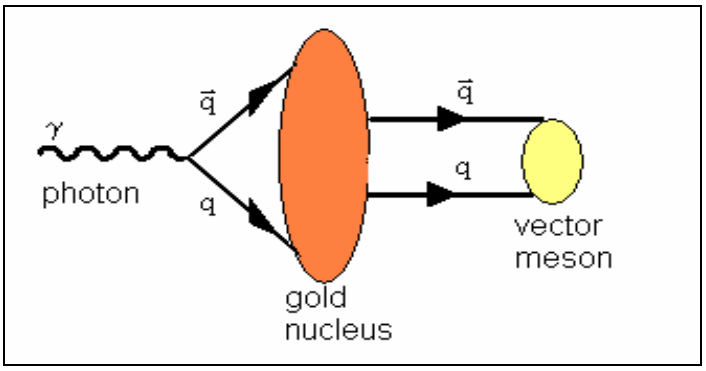

Figure (3.2): Photonuclear interactions. In photonuclear interactions, a photon emitted by one nucleus fluctuates into a quark-antiquark pair. When this pair scatters from a nucleus, a neutral vector meson emerges.

(3.4) Pomeron-Pomeron Interactions:

If the impact parameter, b, is approximately 2R (grazing collisions), the two nuclei can interact via strong interactions. These are known as Pomeron-Pomeron interactions. The Pomeron is considered a virtual particle that carries the strong force, colorless and having the quantum numbers of the vacuum. However, the exact nature of the Pomeron is still unknown. Studying these interactions will provide information about how Pomerons interact with nuclei.

The three types of interactions described above can be coherent interactions. In coherent interactions, each nucleus interacts as a whole, which results in a source of photons large compared to the individual protons or neutrons inside the nucleus. The wavelength of an object depends on the size of its source: the larger the size of the source, the larger the wavelength of the emitted particles. As a result of this relatively large source, the emitted photons have relatively large wavelengths (λ) and therefore

relatively small momenta (p) since $p = h/\lambda$, where h is Planck's constant. Since the transverse component of the momentum comes from exchanged particles, p_T is small. This small transverse momentum is a clear experimental signature of a coherent interaction.

(3.5) The Ultra Peripheral Collisions Program In STAR:

Initially STAR focused on observing ρ^0 production because it would be detected with the highest rate. We now extend the search to more exotic mesons. Physicists are interested in these interactions since these studies help to determine quark structures of "exotica"; particles that are made in whole or in part by gluons. We also study photon-photon interactions such as e^+e^- production. My study will focus on photonuclear vector meson production.

CHAPTER 4

EXPERIMENTAL EVIDENCE FOR X (1750) MESON

Photoproduction experiments have observed an enhancement in the K^+K^- mass spectrum near 1.75 GeV/c^2 [7-9]. This enhancement was identified as the ϕ (1680), a radial excitation of the ϕ (1020). Using the FOCUS spectrometer with photon beam energies between 20 and 160 GeV, the FOCUS collaboration at Fermi National Accelerator Laboratory confirmed the existence of the photoproduction enhancement in K^+K^- at 1.75 GeV/c^2, but their results challenge the interpretation of this enhancement as the ϕ (1680). This chapter discusses the experimental evidence for the enhancement in the K^+K^- mass spectrum near 1.75 GeV/c^2.

(4.1) OMEGA Collaboration:

The reaction $\gamma p \rightarrow K^+K^- p$ was studied at the CERN –SPS using the Omega spectrometer with photons in the energy range 20-70 GeV.[7] A schematic diagram of the Omega spectrometer is shown in Figure (4.1). The incident photon beam is focused on the center of a hydrogen target, which is placed inside a magnetic field of 0.9T. The detector system includes multiwire chambers, which are used in the trigger, drift chambers that provide measurements of particle trajectories, a large threshold Cherenkov counter and a photon detector. The Cherenkov counter is used to identify particles, using their threshold momenta. The threshold momentum is the minimum momentum a given particle must have to begin producing a light signal in the Cherenkov detector. In this experiment, the Cherenkov counter is filled with carbon dioxide at atmospheric pressure.

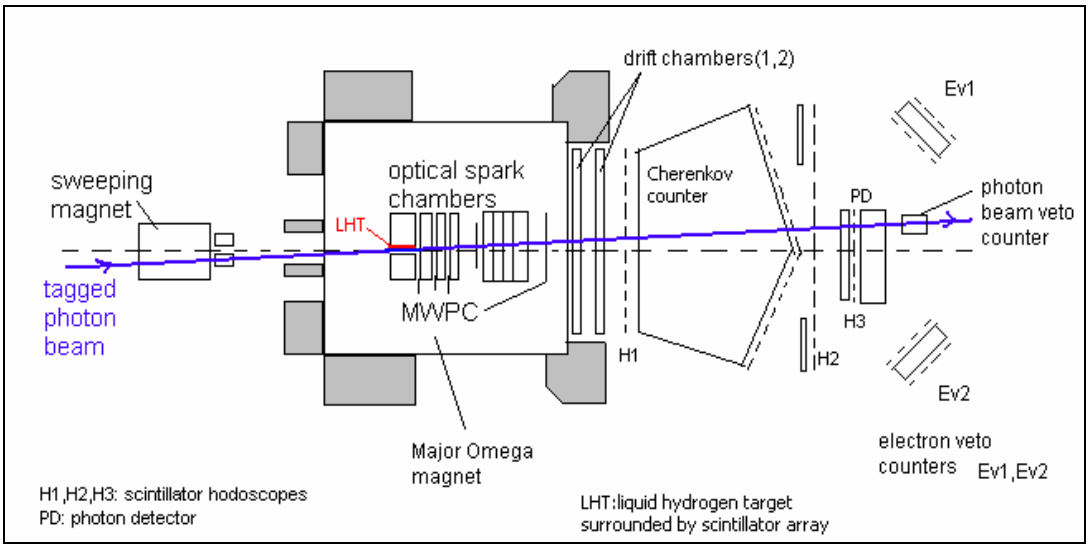

Figure (4.1): Side view of the Omega spectrometer. The detector system includes a liquid hydrogen target, multiwire proportional chambers (MWPC), drift chambers, and a Cherenkov counter.[7]

CO_2 is chosen so that charged particles with momenta between 5.6 GeV/c and 17 GeV/c begin to radiate Cherenkov light and can be identified as kaons or protons[7,10]. Since the investigated reaction is $\gamma p \rightarrow K^+K^- p$, events with two or three charged tracks which come from a single vertex were studied. In order to study this reaction, all other reactions that can produce three charged particles have to be eliminated. In this experiment, there are 3 major background events; $\gamma p \rightarrow e^+e^- p$, $\gamma p \rightarrow \pi^+\pi^- p$ and $\gamma p \rightarrow p\ \bar{p}\ p$. Figure (4.2a) shows the K^+K^- mass spectrum for all events which yield three charged particles after eliminating these background events. Figure (4.2b) shows the mass spectrum for only those events in which both kaons are identified.

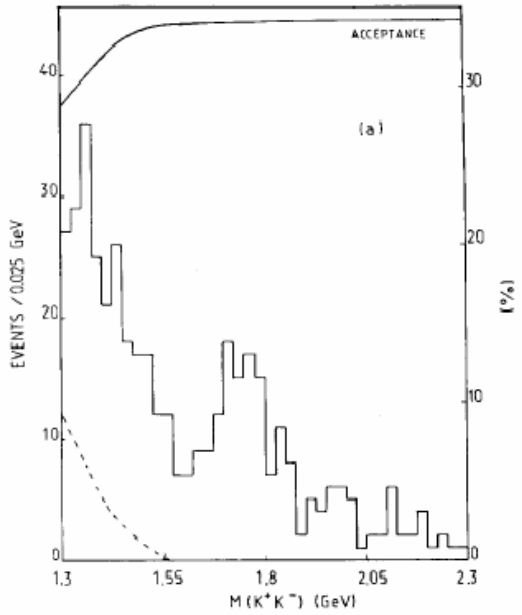

Figure (4.2a): Mass distribution for all events of $\gamma p \rightarrow K^+K^-p$. This shows the mass distribution for all events which yield three charged particles. The dotted line shows the background events.[7]

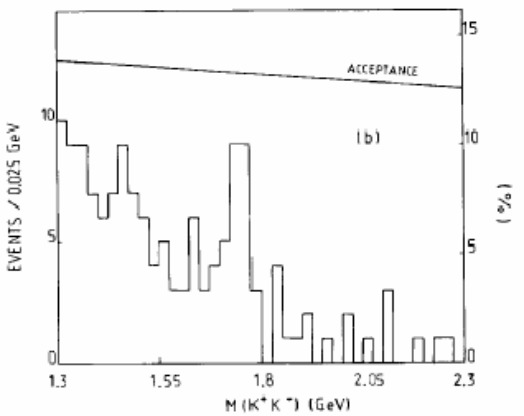

Figure (4.2b): Mass distribution for two kaon candidates. This shows the mass distribution for the events of the type $\gamma p \rightarrow K^+K^-p$, where both kaons are identified.[7]

In both spectra a resonance near 1.75 GeV/c^2 can be seen. By fitting the resonance to a Briet-Wigner distribution, the mass was determined to be 1.69 ± 0.01 GeV/c^2, and the width was 0.10 ± 0.04 GeV/c^2. The cross section for this reaction was determined to be 8 ± 3 nb. These results are compatible with the results for ϕ (1680) [11]. With these results, the OMEGA Collaboration presented evidence for a vector meson at a mass of 1.69 GeV/c^2 decaying into K^+K^-.

(4.2) FNAL E401 Collaboration

The E401 collaboration at Fermi National Laboratory, Illinois, studied elastic photoproduction on deuterium in the energy range 45-85 GeV[8]. In this experiment, photons originating from the decay of π^0, produced by a beam of 350 GeV protons, were focused on a beryllium target. The ratio of photons to neutral hadrons was enhanced by passing the neutral beam through a liquid deuterium filter. The resulting neutral beam was approximately 99% photons. The remaining 1% consisted primarily of K_L^0. Two concentric rings of scintillator counters were placed surrounding the target for recoil detection. Momentum measurements were taken by using a system of multiwire proportional chambers and two analyzing magnets. Two multicell Cherenkov counters with π, K, p thresholds of 5.9, 20.9, 39.7 GeV/c and 10.7, 37.8, 71.9 GeV/c were used for hadron identification. (These are the momentum values at which pions, kaons and protons begin to radiate Cherenkov light.)

The following cuts were imposed to select possible high mass states decaying into K^+K^- pairs: (1) selected events were required to have two oppositely charged tracks that extrapolated back to a common vertex, (2) each track had to have signals in both Cherenkov counters that were consistent with the signals of kaons, and (3) each track had to have a signal in at least one Cherenkov counter that was much smaller than the signal left by a pion of the same momentum. This last cut eliminated 90% of the signal expected from pions. Similarly, protons were eliminated by selecting events such that at least one track had a signal much greater than the signal left by a proton. After subtracting the background, figure (4.3) shows the mass distribution of K^+K^-. A clear enhancement near 1.7 GeV/c^2 can be seen. The mass and the width of the enhancement obtained assuming a

Breit-Wigner distribution are 1.726 ± 0.022 GeV/c^2 and 0.121±0.047 GeV/c^2 respectively. The cross section is 8.0 ± 2.7 nb. Since these results are consistent with the results of the OMEGA Collaboration photoproduction experiment, the enhancement was identified as ϕ (1680), a radial excitation of ϕ (1020).

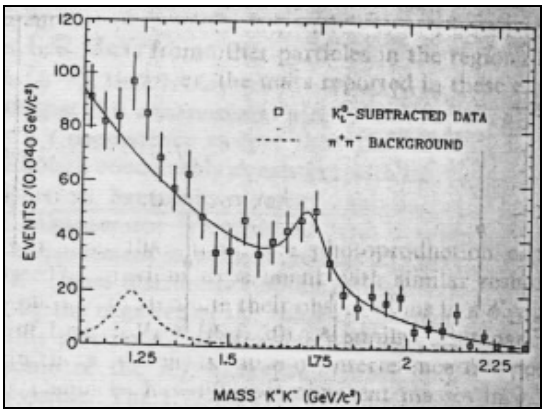

Figure (4.3): K^+K^- mass distribution. This shows the K^+K^- mass distribution after subtracting K^0_L events. A clear enhancement at 1.7 GeV/c^2 can be seen. The dotted line comes from misidentified $\pi^+\pi^-$ [8].

(4.3) FOCUS Collaboration:

During the Fermi National Accelerator Laboratory 1996-1997 fixed-target run, the FOCUS Collaboration studied the interactions of high-energy photons on a BeO target[9]. They used the FOCUS spectrometer with photon beam energies between 20 and 160 GeV. Figure (4.4) shows a schematic diagram of the FOCUS spectrometer. A photon beam is produced from the bremsstrahlung of secondary electrons and positrons produced from the proton beam. The charged particles that emerge from the target are tracked by two systems of silicon microvertex detectors. These detectors provide high resolution separation of primary (production) and secondary (decay) vertices. The momentum of a charged particle is determined by measuring its deflection in two

magnets with opposite polarity. Three threshold Cherenkov counters are used to identify pions, kaons and protons. The K^+K^- data used in the experiment are selected to be events that have two oppositely charged tracks and a single vertex in the target. Events with additional reconstructed tracks are rejected. The mass spectrum of K^+K^- shows a clear $\phi(1020)$ signal in Figure (4.5).

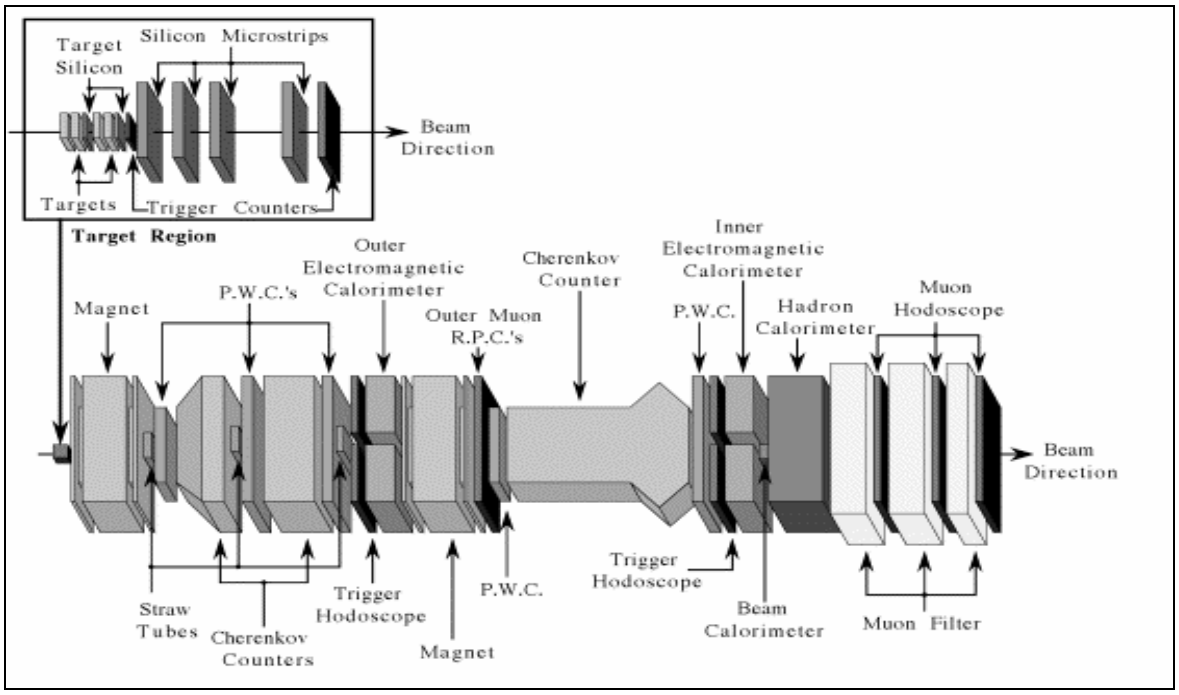

Figure (4.4): A schematic drawing of the FOCUS spectrometer. The target region consists of a BeO target, two silicon microvertex detectors and trigger counters. Three Cherenkov counters are used to identify electrons, pions, kaons and protons[13].

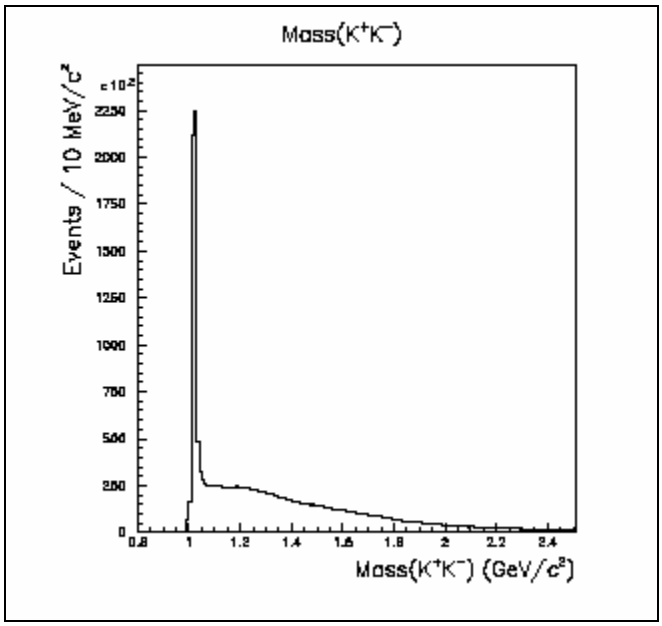

Figure (4.5): The K^+K^- mass spectrum with no cut on p_T. The K^+K^- sample, with two oppositely charged tracks and a single vertex, shows a clear $\phi(1020)$ signal[9].

In the p_T spectrum shown in Figure (4.6), the diffractive (coherent) component of the production of $\phi(1020)$ can be seen as a peak at low p_T, near 0.1 GeV/c^2.

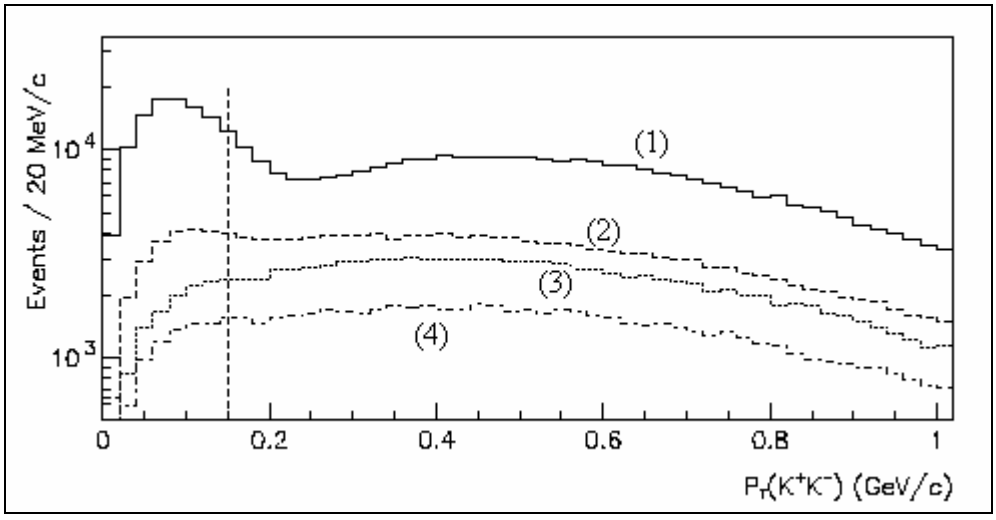

Figure (4.6): The K^+K^- p_T spectra. The solid line (1) is the p_T spectrum for the $\phi(1020)$. Line (2) is the p_T spectrum for K^+K^- masses between 1640 and 1860 MeV/c^2. Lines (3) and (4) are for the left side band (1500-1600 MeV/c^2) and for the right side band (1900-2100 MeV/c^2) respectively[9].

Plotting the p_T spectrum in the 1750 mass region, line (2) in Figure (4.6), we see a slight peak at low p_T (< 0.15 GeV/c). This shows there is some diffractive (coherent) production in this region. The p_T spectra of the two side band regions (1500-1600 MeV/c^2 and 1900-2000 MeV/c^2), as seen in lines (3) and (4) in Figure (4.6), do not show a similar peak. This indicates that the background is non-diffractive. The diffractive sample of K^+K^- events was selected with a p_T cut < 0.15 GeV/c. This sample shows a clear enhancement in the mass spectrum near 1.75 GeV/c^2, as seen in Figure (4.7).

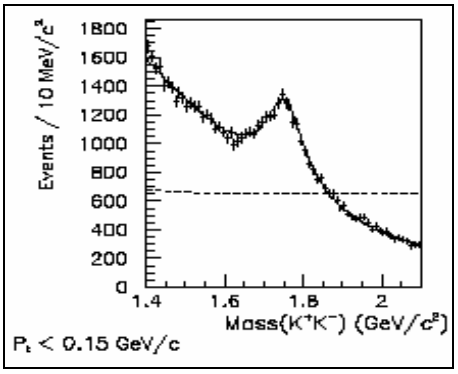

Figure (4.7): The K^+K^- mass spectrum for p_T < 0.15 GeV/c[9].

The FOCUS collaboration made two observations. First, with more than 10,000 signal events and nearly 100 times the statistics of the previously mentioned experiments, the mass of this enhancement is determined as 1.75 ± 0.0015 ± 0.0023 GeV/c^2 , which is clearly inconsistent with the ϕ' (1680). The width is determined as 0.122 ± 0.0062 ± 0.0008 GeV/c^2. Second, although the dominant decay mode of the ϕ (1680) is K^*K, there is no evidence for the enhancement in K^*K corresponding to the enhancement in $K^+ K^-$. Therefore, this enhancement is proposed as a new resonance X (1750).

CHAPTER 5

DATA ACQUISITION

In the RHIC run in 2001 (from August 5 to November 26), gold nuclei were accelerated to an energy of $\sqrt{s}$ = 200 GeV/nucleon. Two main trigger sets, The Production Minimum Bias trigger set and The Production Central Trigger set were used to study ultra peripheral collisions. Triggering is an important part of collecting data. Triggers are used to select interesting signals and to reject background events. This chapter discusses each of the trigger sets used in the year 2001 RHIC run.

(5.1) The Production Minimum Bias Trigger

The Minimum Bias Trigger is based on the east and west Zero Degree Calorimeters (ZDC). Coincident signals are required in both zero degree calorimeters. When bunches from the two gold beams, yellow and blue, overlap with each other at the same time that signals are recorded at both ZDCs, such events are defined as 'Minimum Bias' events and are recorded. These types of collisions are mainly central collisions, where two gold nuclei overlap completely with each other. In ultra peripheral collisions, the exchanged photon which produces the neutral vector meson leaves the nuclei in their ground states. However, the nuclei can exchange an additional photon, which puts them into an excited state as seen in Figure (5.1). These excited nuclei can decay by single or multiple neutron emission. The ZDCs detect these emitted neutrons. Therefore, the Minimum Bias Trigger detects all events whether they are central or ultra peripheral events, without any physics bias.

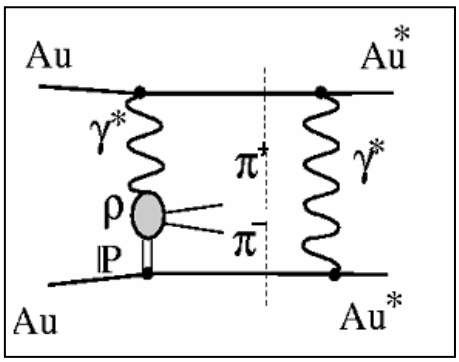

Figure (5.1): An Au-Au collision with nuclear excitation. The process to left of the dashed line shows a collision without nuclear excitation. The process to right of the dashed line is an additional photon exchange. The dashed line indicates the two processes are independent. The excited gold nuclei decay by single or multiple neutron emission, which is detected by the ZDC[14].

Figure (5.2) shows the ZDC signals for ultra peripheral events selected by the Minimum Bias trigger. Most ultra peripheral events selected by Minimum Bias Trigger decay by single neutron emission.

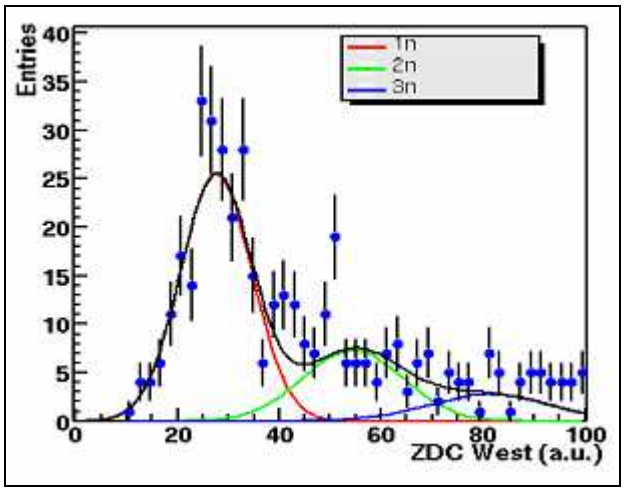

Figure (5.2): ZDC signals with Minimum Bias trigger. Blue dots show data. Red, green and blue lines show one, two and three neutron emissions respectively. The graph shows most ultra peripheral events selected by Minimum Bias Trigger decay by single neutron emission[14].

(5.2) The Production Central Trigger

The Production Central trigger set consists of two main parts: The Central trigger, which contributes ~90% of the data set and the Ultra Peripheral Collisions trigger, which contributes ~10% of the data. The Central trigger is designed to select central collision events. The Ultra Peripheral Collisions trigger is designed to select ultra peripheral collision events.

(5.2.1) The Ultra peripheral Collisions Trigger

The ultra peripheral collisions (UPC) trigger uses the CTB instead of the ZDCs. In this trigger, the central trigger barrel is divided into four regions: top, bottom, north and south, as seen in Figure (5.3). A typical event for ρ (770) meson decay is shown by the dashed line. Since the ρ (770) mesons decay into two oppositely charged pions, we expect to have coincident signals in opposite quadrants. A major background that will satisfy this trigger is cosmic rays. As cosmic rays fall down vertically from outer space, we can reject the cosmic ray background by eliminating signals in the top and bottom quadrants.

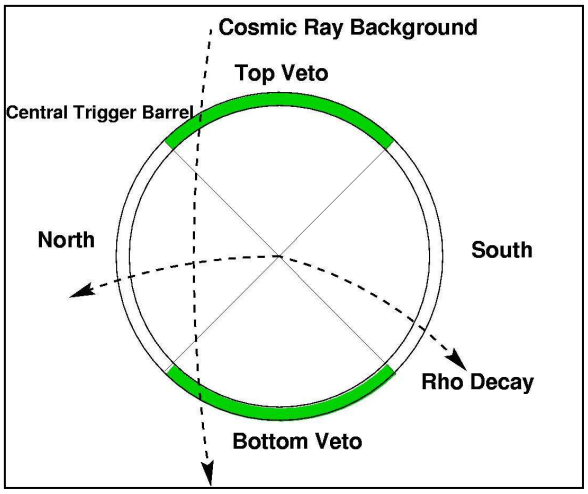

Figure (5.3): Side view of Ultra Peripheral Collisions trigger. The trigger barrel is divided into 4 regions. The typical ρ(770) meson decay is shown by the dashed line.

Only events which produce coincident signals in the north and south quadrants are accepted by this trigger.

The UPC trigger does not place any requirement on ZDC signals, however we can check what the signal is in the ZDCs for UPC triggered events. This is shown in Figure (5.4). The peak near ADC channel 5 is the baseline voltage of the detector. Because there is nothing above 5, no neutrons were emitted. This means that the Minimum Bias trigger and Ultra Peripheral Collisions trigger are based on different physics. The Minimum Bias Trigger detects ultra peripheral events with excited gold nuclei. The Ultra Peripheral Collisions Trigger detects events where gold nuclei remain in their ground state.

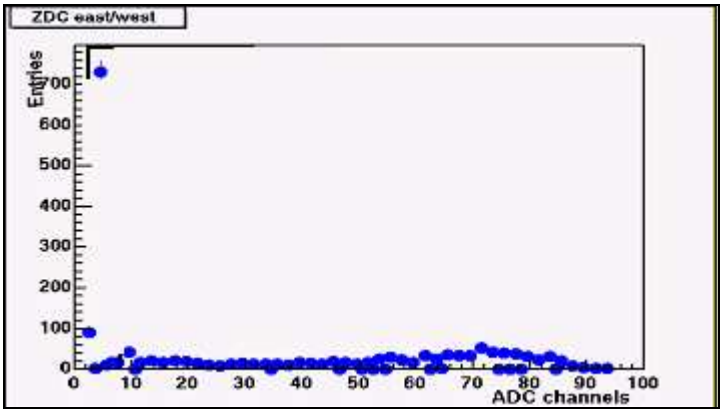

Figure (5.4): ZDC signals with Ultra Peripheral Collisions trigger. Collisions without nuclear excitation are detected. Gold nuclei remain in the ground state.

In the year 2001 RHIC run, two magnetic field strengths were used; the half field strength was 0.25 T and the full field strength was 0.5 T. For my study I used two data sets. One data set was taken with a 0.25 T magnetic field strength and the Minimum Bias Trigger. The other data set was taken with a 0.5 T magnetic field strength and with the Minimum Bias Trigger. The 0.5 T is the maximum field strength that STAR can achieve. Number of events in each data set is shown in Table (5.1).

Minimum Bias Trigger: 0.5T magnetic field strength- Number of events	Minimum Bias Trigger: 0.25T magnetic field strength- Number of events
359207	99204

Table (5.1): Data sets used in this study. Both sets were taken with the Minimum Bias trigger.

CHAPTER 6

DATA ANALYSIS

When a charged particle passes through a gas, free electrons and positive ions are produced along its track due to the ionization of the gas. By applying an electric field, electrons and ions can be collected at the cathode and the anode. The STAR TPC determines the momentum of individual particles and identifies them by making energy loss measurements. The TPC tracks particles through a solenoidal magnetic field, which causes charged particles to move in helical paths. Once the paths of charged particles have been reconstructed, the momentum of the particles can be determined.

(6.1) The momentum of a charged particle in a magnetic field

The centripetal force (F_c) depends on the tangential component of the velocity ($v_\perp$), the mass (m) of the particle, and the radius (r) of the circle:

$$F_c = m v_\perp^{\,2}/r. \qquad (6.1)$$

The force on a particle due to an applied magnetic field B is:

$$\vec{F} = q(\vec{v} \times \vec{B}) = qvB\sin\theta \ . \qquad (6.2)$$

where q is the charge and θ is the angle between the velocity and the field. The field is parallel to the beam line. Since the only radial force applied to the particle is the magnetic force, $\vec{F} = F_c$. Since the particle travels in a helix, the transverse component of velocity (i.e., the velocity component perpendicular to the beam line) $v_\perp = v \sin\theta$.

From (6.1) and (6.2), $m v_\perp / r = qB$.

Therefore, the transverse momentum of the particle $p_T = rqB$. The charge (q) of the particle can be determined by the direction of curvature of its track, as oppositely charged particles curve in opposite directions in a magnetic field. Since the strength of the magnetic field (B) is known and the radius of the curvature (r) can be measured from the reconstructed track, the transverse momentum of the particle can be determined. In the TPC, particles drift towards the end-caps in helical paths. The longitudinal component of momentum can be determined by considering the longitudinal distance traveled in a given time.

(6.2) The energy loss of a charged particle

The rate of energy loss per unit length (dE/dx) of a charged particle due to the ionization in a given medium is given by the Bethe-Bloch formula;

$$-dE/dx = 4\pi N_0 r_e^2 m_e c^2 (Z/A)\rho\left(\frac{1}{\beta^2}\right) q^2 \left[\ln\left(\frac{2m_e c^2}{I} \beta^2 \gamma^2 \right) - \beta^2 - \frac{\delta}{2} \right] . \quad (6.3)$$

In this expression, N_0 is Avogadro's number; $r_e \left(= \frac{e^2}{m_e} \right)$ is the radius of the electron; ρ, Z and A are the density, atomic number, and mass number respectively of the medium; q is the charge of the particle traversing the medium; I is the ionization potential of the medium; δ describes the reduction of the energy loss at highly relativistic velocities; $\beta = v/c$; and $\gamma = \frac{1}{\sqrt{1-\frac{v^2}{c^2}}}$.[15] The TPC is capable of determining the energy loss of particles that pass through the gas. When the energy loss is high, more gas particles are ionized. This causes thicker trails in the drift chamber which give signals with larger magnitudes.

For a given mass, a graph of (dE/dx) versus momentum gives a characteristic curve. Those curves can be used to identify particles, as shown in Figure (6.1). In many regions the curves for different particles are well separated. In these regions particle identification can be done unambiguously.

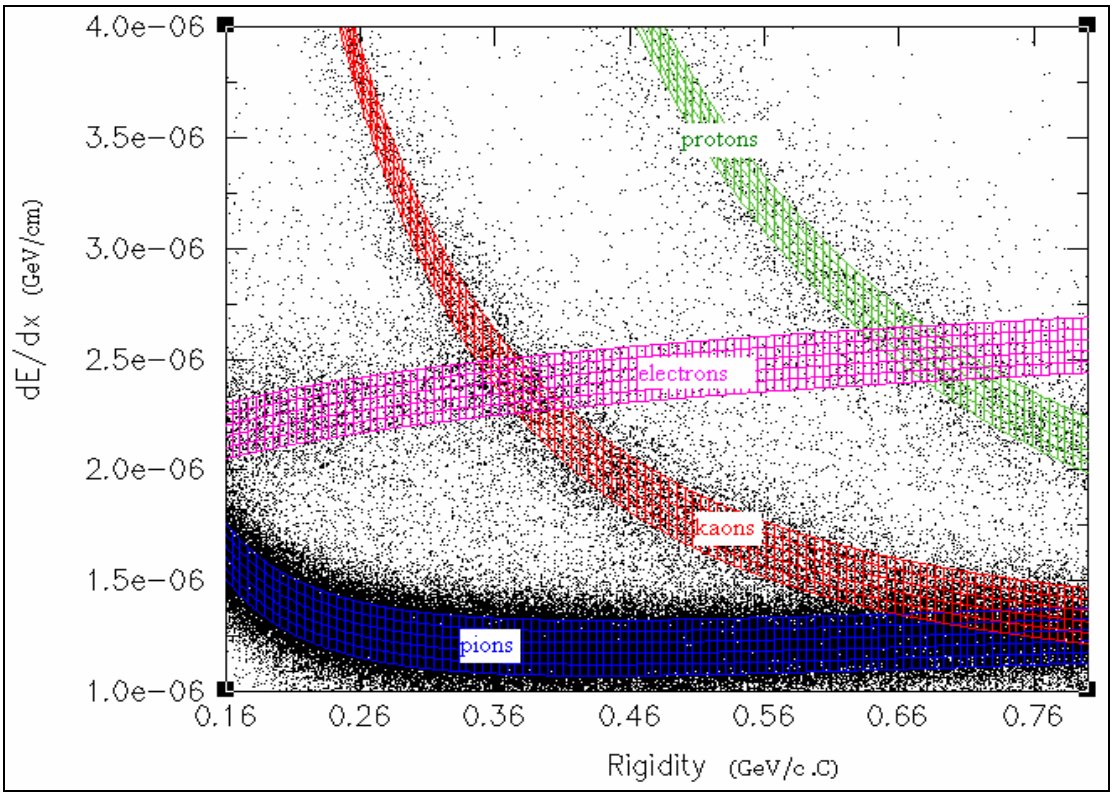

Figure (6.1): The energy loss versus rigidity for different particles. Rigidity is defined as (momentum/charge). The color codes are blue for pions, orange for kaons, green for protons and pink for electrons[16].

For our analysis, rather than using directly the energy loss per unit length (dE/dx), we used the log value of the ratio of measured energy loss to the expected energy loss for kaons calculated from the Bethe-Bloch formula (Equation 6.3).

Log (dEdx/dEdxk) = log (Measured energy loss/Expected energy loss for kaons). This value should be zero for all kaons if the experimental dE/dx measurement is properly calibrated.

(6.3) Meson Spectroscopy

This work studies the interaction $X \rightarrow K^{+}K^{-}$. Because the X (1750) is neutral and short-lived, we observe the kaons, the decay products of X (1750). This section discusses how to study meson production by using their decay products.

The total energy of the decay products should be equal to the energy of the initial particle and the total momentum of the decay products should be equal to the momentum of the initial particle. Using these conservation laws, we can determine the invariant mass of the initial neutral particle.

Example : ρ (770) Meson

The ρ meson decays into two oppositely charged pions ($\rho \rightarrow \pi^{+} + \pi^{-}$) . These charged pions can be observed and therefore their momenta can be measured. Using the equation $E_{\pi}^{2} = p_{\pi}^{2}c^{2} + m_{\pi}^{2}c^{4}$ with the invariant mass of the pion (139.6 MeV) and the measured momentum, the energy of each pion can be calculated. The sum of these energies should be equal to the energy of the initial particle, $E = E_{\pi+} + E_{\pi-}$. The total momentum of the initial particle can be calculated by adding the momenta of the individual pions; $\vec{p} = \vec{p}_{\pi^{+}} + \vec{p}_{\pi^{-}}$. With the total energy and the total momentum, and with the equation $E^{2} - p^{2}c^{2} = m^{2}c^{4}$, the invariant mass of the initial particle can be determined. If the observed mass spectrum of pions matches the expected mass spectrum for ρ meson, it can be concluded that the observed pions are the decay products of a ρ meson.

(6.4) The search for the X (1750)

Since the expected decay mode for X(1750) is $X \rightarrow K^{+}K^{-}$, we are looking for two oppositely charged tracks that come from a single vertex within the interaction region. To select such events we considered the following cuts.

1) The total charge of two tracks should be zero.
2) The vertex is required to be close to the center of the detector in both longitudinal distance (z) and the radial distance (r). This is because the collisions occur at the center of the TPC.
3) The number of tracks should be small. Events of interest to my study should have only two tracks, but in order to have a less restricted data sample, I also considered events with more than two tracks.
4) Each track should be well reconstructed. For this, we consider the number of hits per track. The higher the number of hits per track, the more well-defined the track.
5) Each track should be identified as a kaon through the energy loss per unit length.

(6.4.1) The background

Event pairs that do not have total charge zero are considered as the background. The signal should be in the low momentum region ($p_T < 0.2$ GeV/c); above that region there should be no signal events. We normalize the signal to background in the region where no signal is expected.

(6.4.2) Cut Selection

The following sections show how I varied the values for above-mentioned cuts to select the best choice of cuts. All the graphs in this section are for data taken with the Minimum Bias trigger with 0.25 T magnetic field strength.

(6.4.3) The longitudinal distance of the vertex from the center of the detector (|z|)

The longitudinal distance of the vertex from the center of the detector, z, is shown in Figure (6.2). The Figure (6.3) shows the transverse momentum and the mass distributions for |z| <25 cm, |z| < 50 cm, |z| < 100 cm and |z|< 200 cm. The other cuts remained constant at relatively loose values (number of tracks < 10, r vertex < 25 cm, number of hits per track >10, log (dEdx/dEdxk) >0.2). We can see that for larger z lengths there are more signal events but the signal to background ratio gets smaller. Therefore we chose the cut |z| < 25 cm since it gives the largest signal to background ratio. Choosing |z| < 25 cm is also important to simplify correlating our sample to the luminosity calculations discussed in Chapter 7.

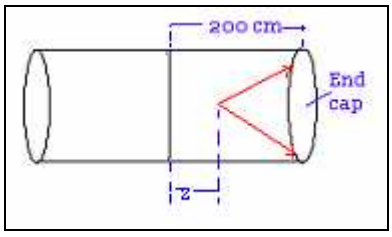

Figure (6.2): The longitudinal distance (|z|) of the vertex from the center of the detector. The maximum z value is 200cm, the distance from the center to the end cap of the drift chamber.

|z| < 25 cm:

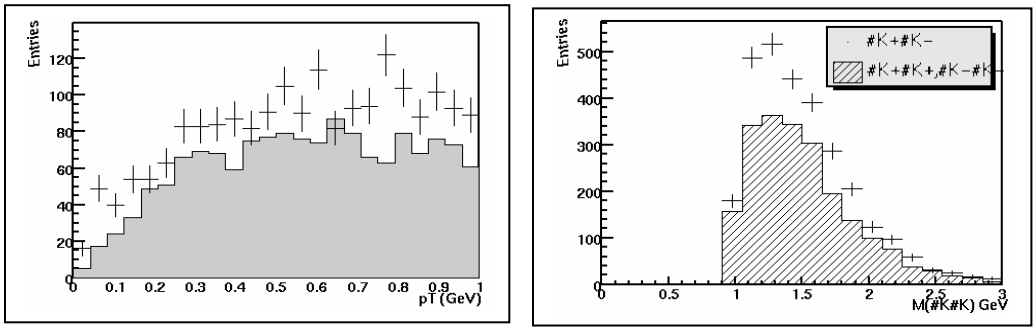

|z| < 50 cm:

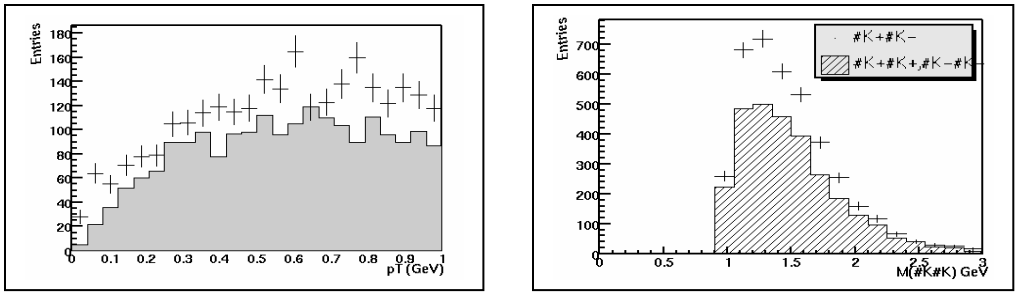

|z| < 100 cm:

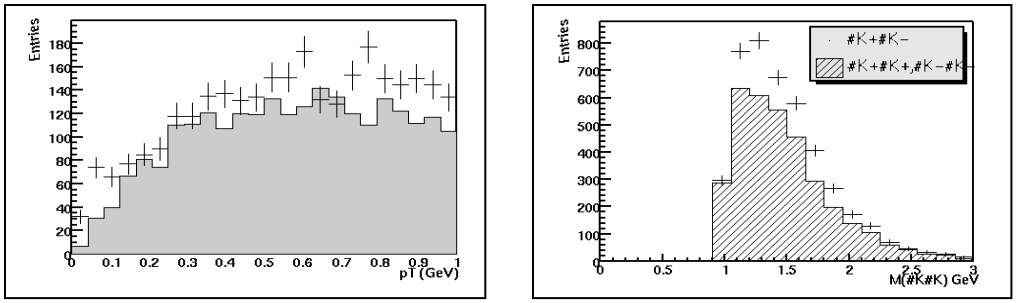

|z| < 200 cm:

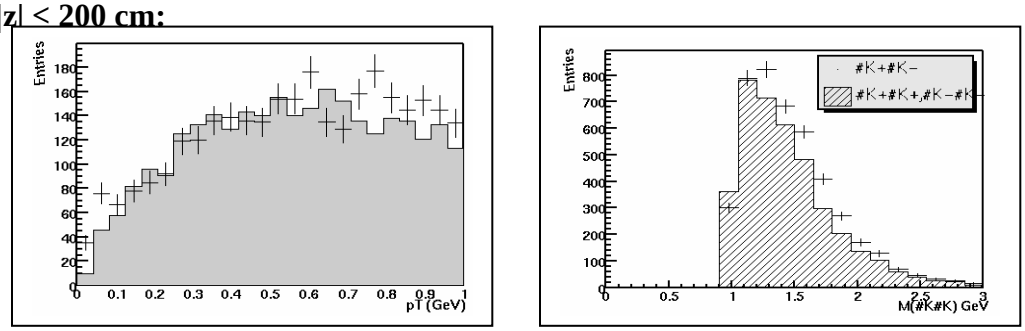

Figure (6.3): The transverse momentum and the mass distribution for different z vertex values. The left column shows the transverse momentum distributions for two kaon candidates for different z values. The gray area shows the background. The right column shows the mass distributions for two kaon candidates for different z values. The lined histogram is for background events.

(6.4.4) The radial distance of the vertex from the beam line (r)

Figure (6.4) shows the radial distance (r) of the vertex from the beam line. Figure (6.5) shows the transverse momentum and the mass distribution for r < 5 cm, r < 15, and r < 20 cm. The other cuts remained constant at relatively loose values (z < 200 cm, number of tracks < 10, number of hits per track > 10 and the log(dEdx/dEdxk) > 0.2). We can see that the variation of the radial distance of the vertex from the beam line does not affect the transverse distribution or the mass distribution of kaons. Therefore we chose to use r vertex < 5 cm.

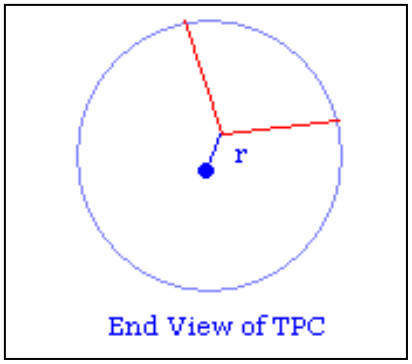

Figure (6.4): The radial distance (r) of the vertex from the beam line.

r < 5 cm:

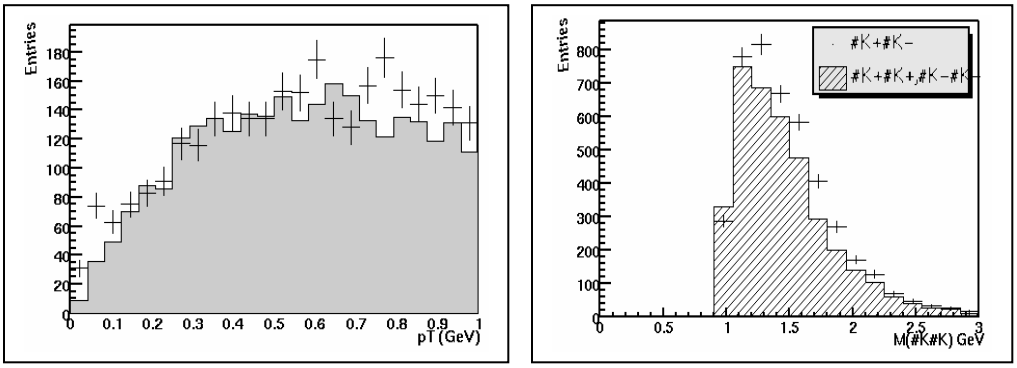

r < 15 cm:

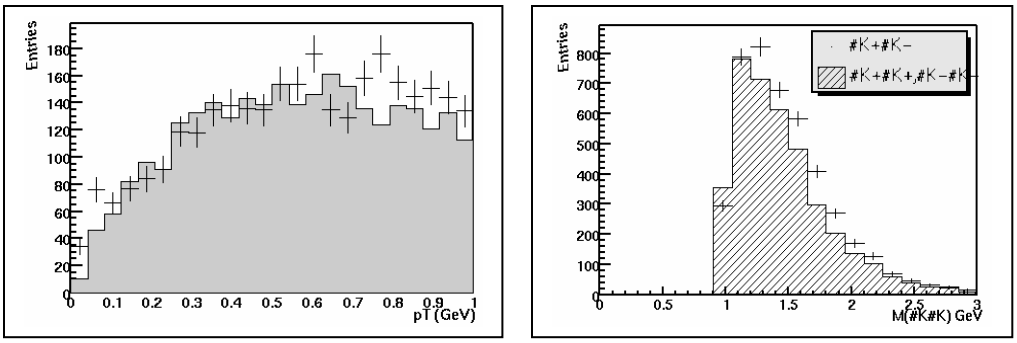

r < 20 cm:

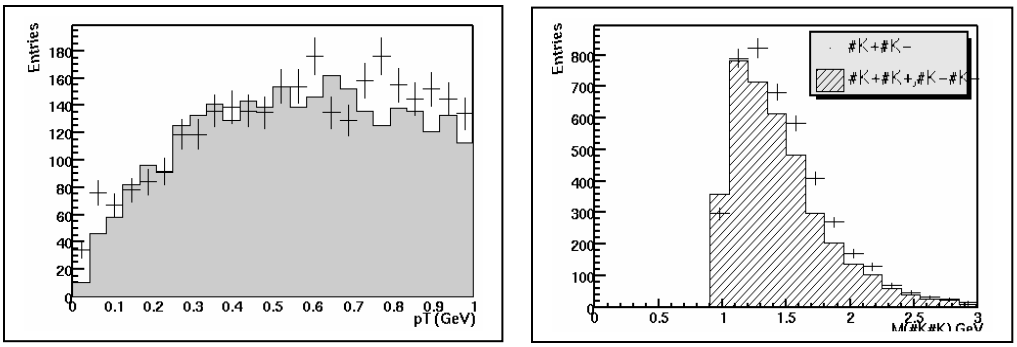

Figure (6.5): The transverse momentum distribution and the mass distribution for different r vertex values. The left column shows the transverse momentum distributions for two kaon candidates for different r values. The gray area shows the background. The right column shows the mass distributions for two kaon candidates for different r values. The lined histogram is for background events.

(6.4.5) The variation of the minimum number of hits per track

Figure (6.6) illustrates hits in the TPC; these hits are used to reconstruct tracks. The more hits along a track, the more accurately the track is reconstructed. Figure (6.7) shows the transverse momentum and the mass distributions when the minimum number of hits is greater than 10, 15, 20 and 25. The other cuts remained constant at relatively loose values (z vertex < 200 cm, r vertex < 25 cm, the log(dEdx/dEdxk) > 0.2 and the number of tracks < 10). We can see that as we increase the minimum number of hits per track, both the signal and the background decrease while the ratio of signal to background does not change significantly. To maximize the signal events, here we chose the minimum number of hits per track to be greater than 10 as the cut.

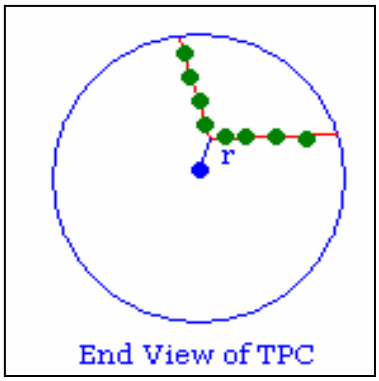

Figure (6.6): The number of hits per track. The black dots represent hits in the TPC. Tracks are reconstructed by connecting the hits.

Number of hits > 10:

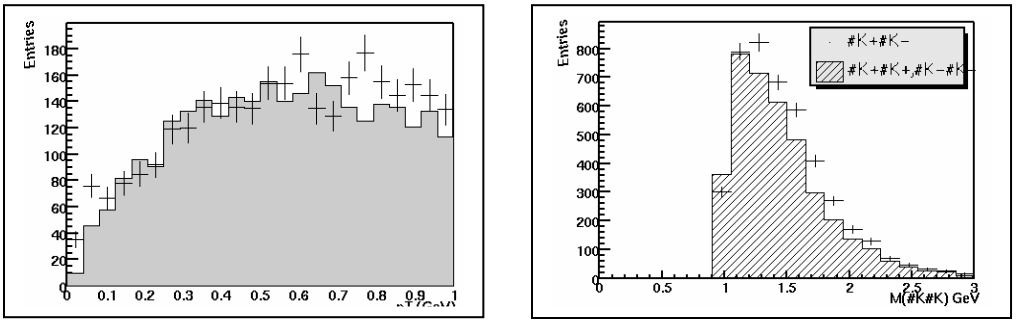

Number of hits > 15:

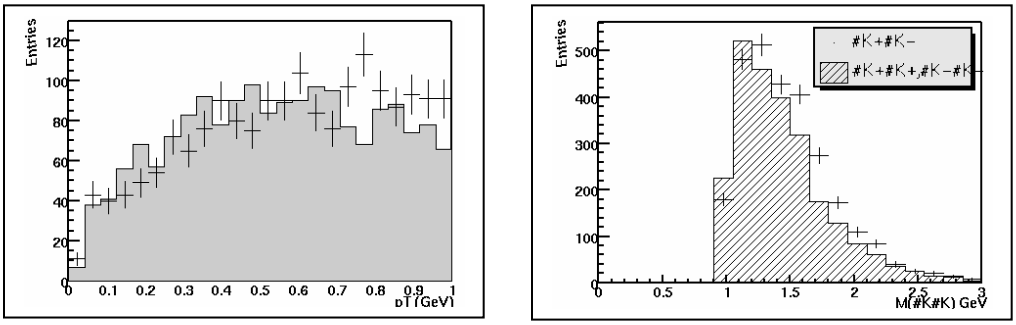

Number of hits > 20:

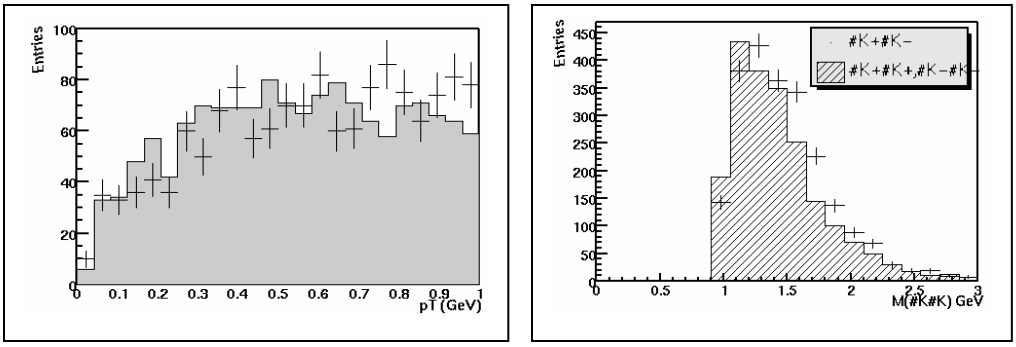

Number of hits > 25:

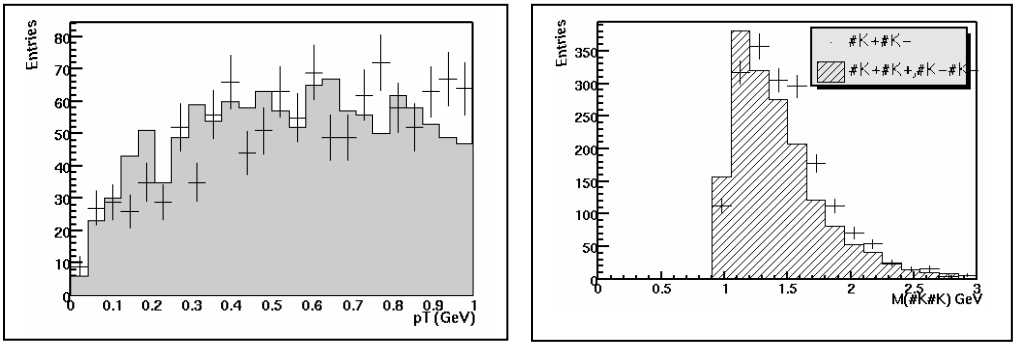

Figure (6.7): The transverse momentum distribution and the mass distribution for different number of hits. The left column shows the transverse momentum distributions for two kaon candidates for different number of hits. The gray area shows the background. The right column shows the mass distributions for two kaon candidates for different number of hits. The lined histogram is for background events.

(6.4.6) The variation of the maximum number of tracks

In this section we show the transverse momentum distribution and the mass distribution for two kaon candidates varying with the maximum number of tracks in the events. In all cases, two particles are required to point back the vertex. Extra tracks are allowed, as they may come from unrelated processes. Figure (6.8) illustrates these tracks in the TPC. Figure (6.9) shows the transverse momentum and the mass distributions for number of tracks less than 3, 5 and 10. The other cuts remained constant at relatively loose values (z vertex < 200cm, r vertex < 25 cm, number of hits per track > 10 and the log(dEdx/dEdxk) > 0.2). We can see that as the maximum number of tracks is increased, both the signal and the background increase but the signal to background ratio decreases. Therefore here we chose the number of tracks to be less than 3.

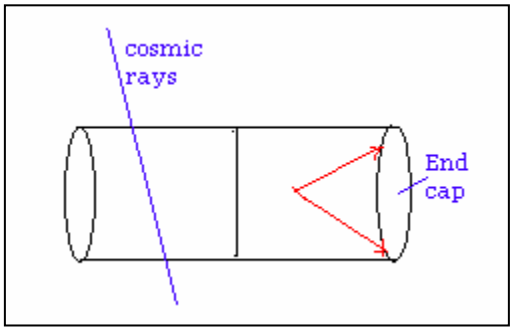

Figure (6.8): The number of tracks. Two particles are required to point back the vertex. Extra tracks are allowed as they may come from unrelated processes such as cosmic rays.

Number of tracks < 3:

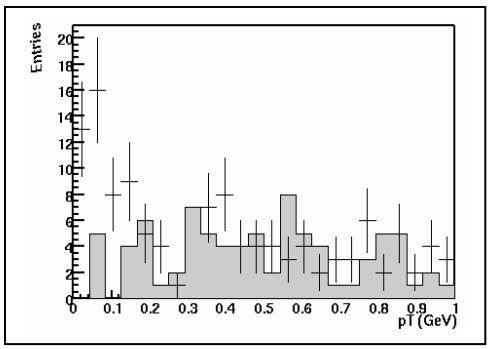

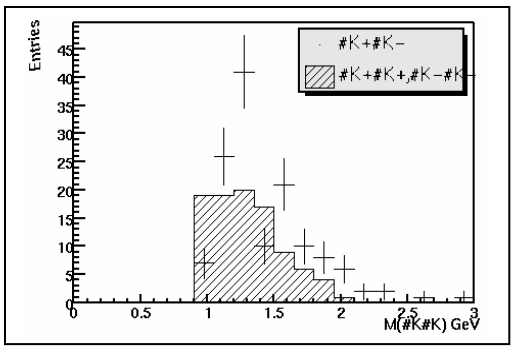

Number of tracks < 5:

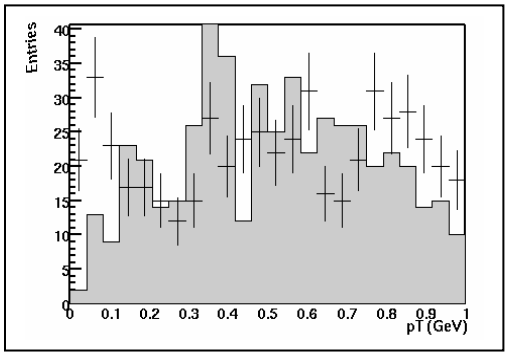

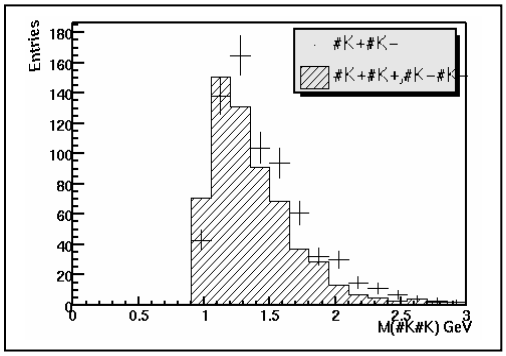

Number of tracks < 10:

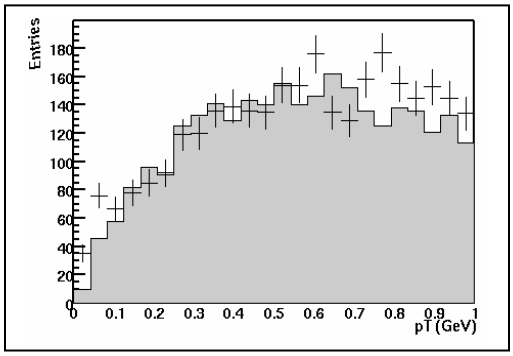

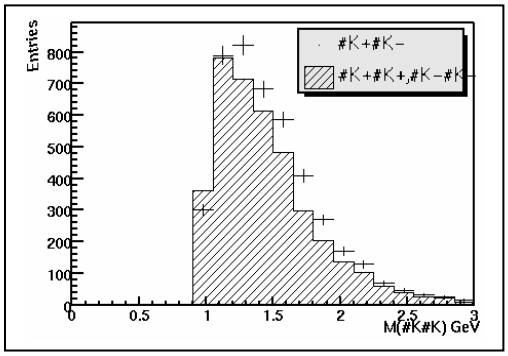

Figure (6.9): The transverse momentum distribution and the mass distribution for different number of tracks. The left column shows the transverse momentum distributions for two kaon candidates for different number of tracks. The gray area shows the background. The right column shows the mass distributions for two kaon candidates for different number of tracks. The lined histogram is for background events.

(6.4.7) The variation of the kaon identification cut

Figure (6.10) shows the distribution of log(dEdx/dEdxk) vs momentum for data taken with the Minimum Bias trigger with 0.25 T magnetic field strength. The kaon band should form a horizontal band around y = 0 in the plot; the fact that this band is a little above zero means that the calibration is not perfect.

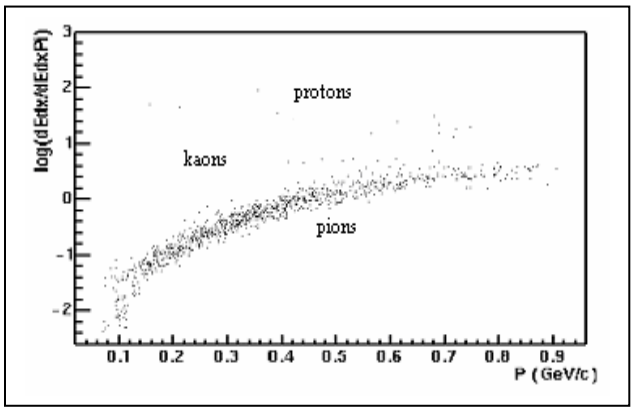

Figure (6.10): The energy loss for events with two primary tracks. This graph is for the data set taken with the Minimum Bias trigger and 0.25 T magnetic field strength. The data set is dominated by pions.

We used two different methods to select kaons. In the first method, we selected a triangular region where kaons are fairly cleanly separated from other particles. Figure (6.11) shows this region.

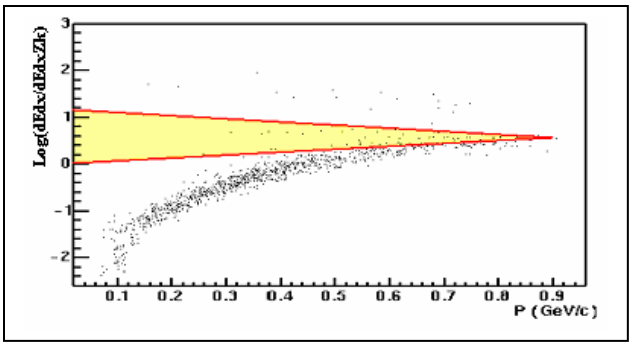

Figure (6.11): Triangular region for filtering kaons. A triangular region is selected to filter kaons from other particles. At momentum >0.9 GeV/c, the kaon and pion bands overlap.

For events with both tracks inside the triangular region, the transverse momentum distribution and the mass distribution are shown in Figure (6.12).

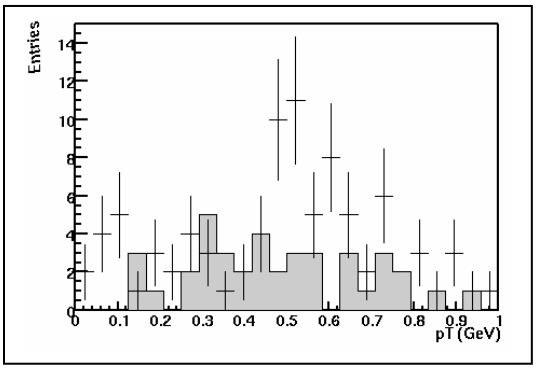

Figure (6.12a): The transverse momentum distribution for kaons inside the triangular region. Both events are identified as kaons. The gray histogram shows the background.

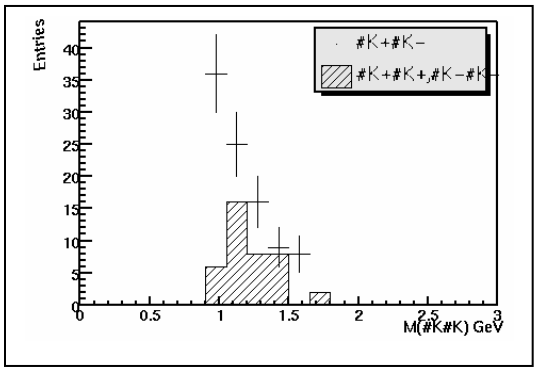

Figure (6.12b): The mass distribution for kaons inside the triangular region. Both events are identified as kaons. The lined histogram shows the background.

In the second method of kaon identification, I considered all the particles with log (dEdx/dEdxk) above some value to be kaons, as shown in Figure (6.13).

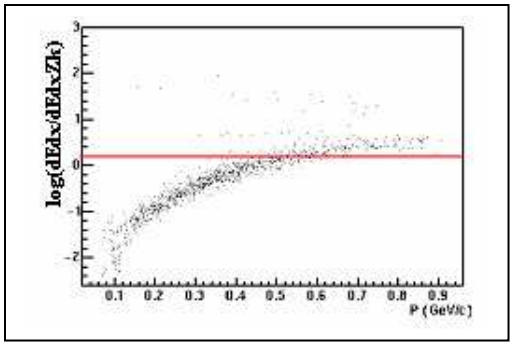

Figure (6.13): The energy loss for two kaon candidates. This graph is for the data set taken with the Minimum Bias trigger and 0.25 T magnetic field strength. All events above the red line (log(dEdx/dEdxk) > 0.2) are considered to be kaons.

With a cut of this type, we can select all the kaons regardless of momentum, but the sample will not be pure. This section discusses how the variation of the value of this cut affects the transverse momentum distribution and the mass distribution of kaons. Figure (6.14) shows the transverse momentum and the mass distributions for log (dEdx/dEdxk) greater than 0.2, 0.3, 0.4, and 0.5. The other cuts remained constant at relatively loose values (z vertex < 200 cm, r vertex < 25 cm, the number of hits > 10 and the number of tracks < 10). For this method of kaon identification, we chose the cut log(dEdx/dEdxk) > 0.2 since it gives the greatest signal to background ratio.

Log (dEdx/dEdxk) > 0.2 :

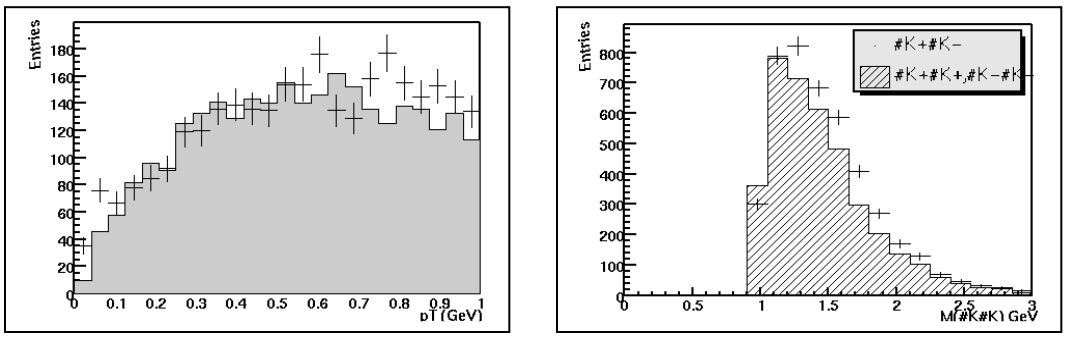

Log (dEdx/dEdxk) > 0.3:

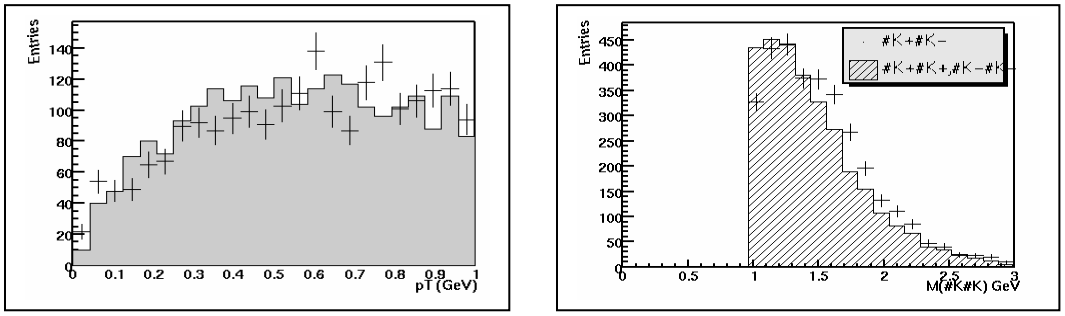

Log (dEdx/dEdxk) > 0.4:

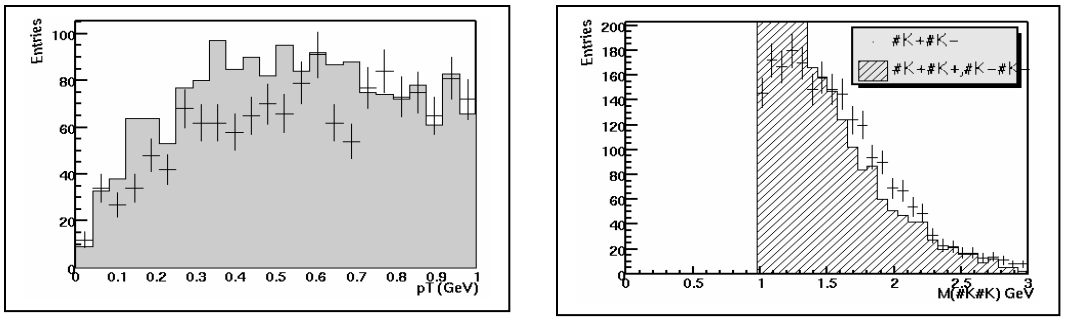

Log (dEdx/dEdxk) > 0.5:

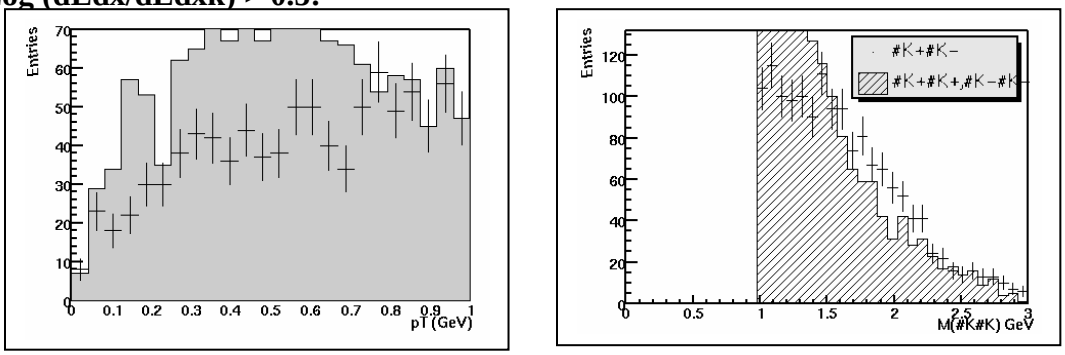

Figure (6.14): The transverse momentum distribution and the mass distribution for different log (dEdx/dEdxk) values. The left column shows the transverse momentum distributions for two kaon candidates for different log (dEdx/dEdxk) values. The gray area shows the background. The right column shows the mass distributions for two kaon candidates for different log (dEdx/dEdxk) values. The lined histogram is for background events.

The first method of kaon identification gives a fairly clean sample, but there are very few events that satisfy the event selection criteria and they are restricted in momentum. The second method of kaon identification gives more events to study with no momentum bias, but the data is less clean. To maximize our sample, we chose the second method of kaon identification, i.e., we selected all particles above the value log (dEdx/dEdxk) > 0.2 to be kaons.

(6.4.8) Values selected for cuts

After studying the effect of varying each of the cuts, we chose the following cuts for our analysis: z vertex < 25 cm, r vertex < 5 cm, the number of hits per track > 10, log (dEdx/dEdxk) > 0.2 and the number of tracks < 3.

CHAPTER 7

RESULTS

This chapter discusses the results obtained with the event selection criteria described in Chapter 6 for the data from the year 2001 RHIC run. Results for the 0.25 T and 0.5 T magnetic field strength data sets are discussed separately. In both cases, if the observed kaons come from decay of the X (1750), we expect to see a peak in the mass distribution of kaons near 1.75 GeV/c^2. Since the X (1750) is coherently produced, we would expect these events to have low net transverse momentum.

(7.1) Data for 0.25 T Magnetic field strength with the Minimum Bias trigger

For data with the 0.25 T magnetic field strength, the transverse momentum distribution is shown in Figure (7.1.1). There is a peak in the low transverse momentum region (< 0.15 GeV). This indicates some of the kaons may come from coherent production. However, the mass distribution does not show a significant peak around 1.75 GeV. Refer to Figure (7.1.2a) and Figure (7.1.2b).

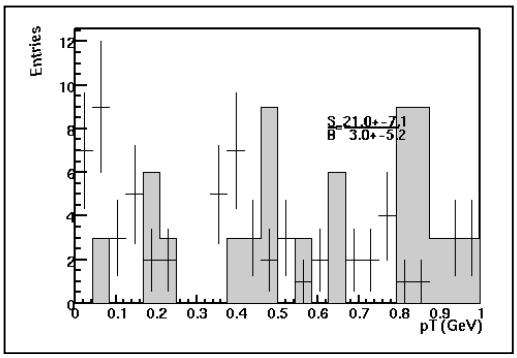

Figure (7.1.1): The transverse momentum distribution for two identified kaons. The gray histogram shows the background events.

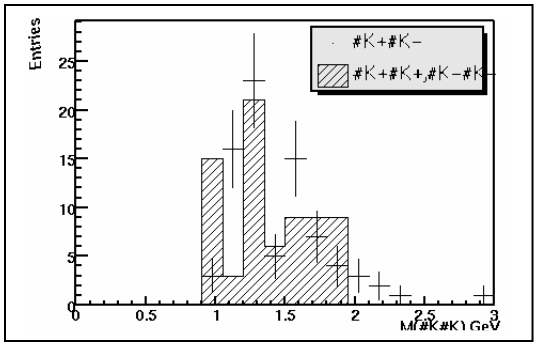

Figure (7.1.2a): The mass distribution for two identified kaons. The lined histogram shows the background events.

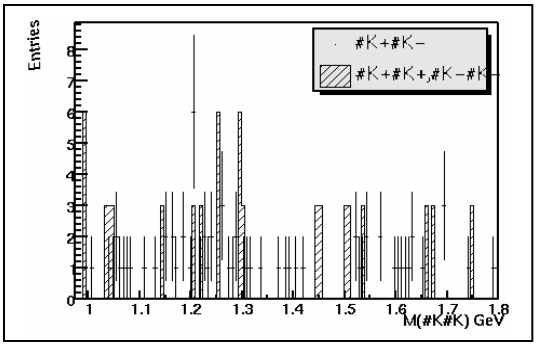

Figure (7.1.2b): The expanded mass distribution for two identified kaons. This is for the region 0.975-1.8 GeV. There is no clear resonance near 1.75 GeV.

Because we expect the kaons from coherent X (1750) production to have a small total transverse momentum, we restrict the mass distribution to only those events with $p_T <$ 0.15 GeV/c to see if this helps select the events of interest. Figure (7.1.3) shows the mass distributions for events with $p_T < 0.15$ GeV/c. This cut removes almost all of the background, indicating the background is non-coherent as expected. We can see that there is still no peak around 1.75 GeV/c^2.

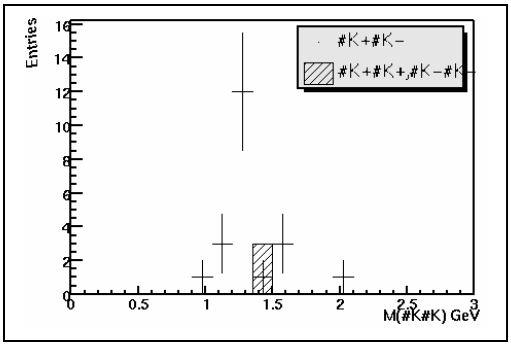

Figure (7.1.3a): The mass distribution for two identified kaons with $p_T < 0.15$ GeV/c. This shows that the background comes mainly from incoherent events.

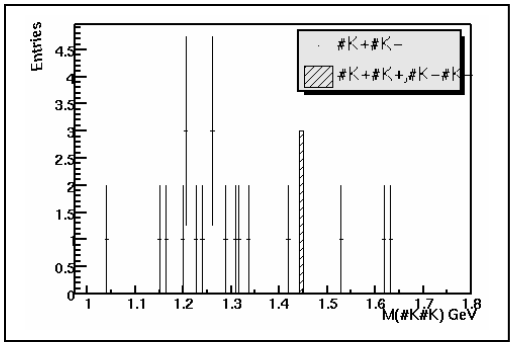

Figure (7.1.3b): The expanded mass distribution with $p_T < 0.15$ GeV/c. There are no coherently produced events near 1.75 GeV.

(7.2) Data for 0.5 T Magnetic field strength with the Minimum Bias trigger

There is much more data taken with the 0.5 T magnetic field than with the 0.25 T magnetic field (359,207 versus 99,204), but many of the features are similar. The transverse momentum distribution for data taken with the 0.5 T magnetic field is shown in Figure (7.2.1). As with data taken with the 0.25 T magnetic field, there is a peak in the low transverse momentum region, indicating some coherent production. Also similar to the data taken with 0.25 T magnetic field, the mass distribution does not show a significant peak around 1.75 GeV/c^2, as shown in Figure (7.2.2).

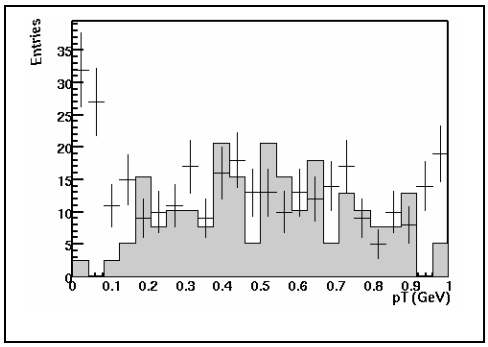

Figure (7.2.1): The transverse momentum distribution for two identified kaons. The gray histogram shows the background events.

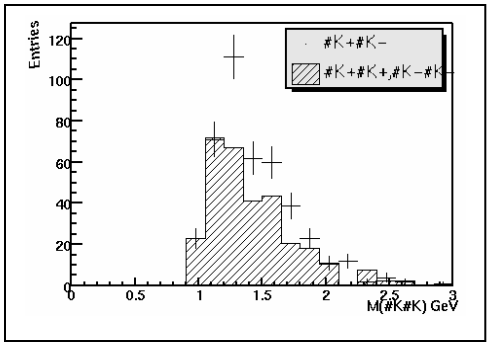

Figure (7.2.2a): The mass distribution for two identified kaons. The lined histogram shows the background.

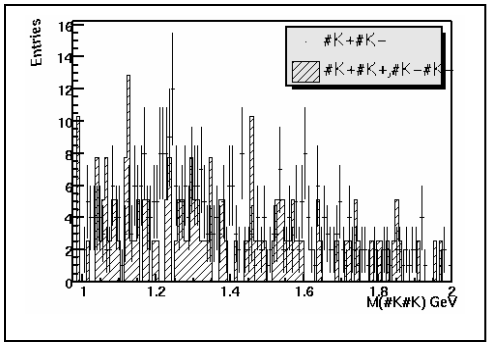

Figure (7.2.2b): The expanded mass distribution for two identified kaons. There is no clear resonance near 1.75 GeV.

As with data taken with the 0.25 T magnetic field, I select events with low p_T (< 0.15 GeV/c) in order to focus on coherently produced kaons. Figures (7.2.3a) and (7.2.3b) show the mass distribution for events with $p_T < 0.15$ GeV/c. In the expanded mass distribution, there are 4 events in the region of interest (1.75 ± 0.122 GeV/c^2), but there is not a significant peak. While we cannot rule out that these may be X (1750) events, there are too few events to make a definitive claim one way or the other.

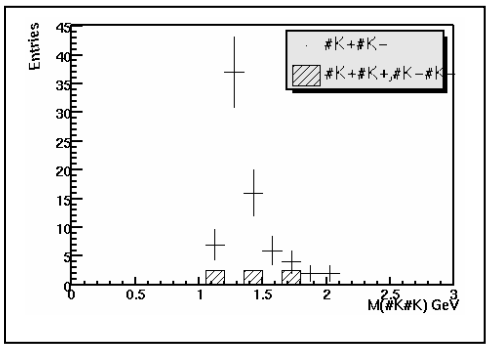

Figure (7.2.3a): The mass distribution for two identified kaons with $p_T < 0.15$ GeV/c. This shows that the background mainly comes from incoherent events.

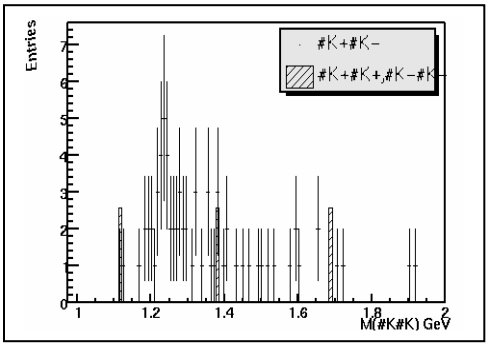

Figure (7.1.3b): The expanded mass distribution with $p_T < 0.15$ GeV/c. There are 4 events in the region of interest.

(7.3) Cross section calculations for X (1750)

The cross section is the "effective cross-sectional area" for a given interaction which is given in units of area: barns (1 barn = 10^{-24} cm^2). A bigger cross section means an interaction is more likely to occur. In this study, due to low statistics, only an upper limit for the cross section can be calculated. The event yield from a particular interaction can be given by the following formula.

Event yield = Acceptance × Integrated Luminosity × Cross section (7.1)

where the event yield is the number of events we observe and the acceptance is the fraction of events which are detected by the detector. The luminosity is the number of

particles in the beam per area per time; the integrated luminosity has been integrated over time to give the number of Au-Au particles in the beam per unit area. The cross section for X (1750) $\rightarrow K^{+}K^{-}$ production in ultra peripheral collisions at RHIC can be measured by observing the event yield.

(7.3.1) Luminosity

The luminosity is the number of particles per square-centimeter per second present in the beams of the RHIC ring. The higher the luminosity, the greater the number of events produced. To calculate the luminosity of ultra peripheral events, we consider the total cross section for hadronic events for the collisions of gold nuclei at RHIC. This value has been determined to be 7.2 barns[17]. Events with more than 7 negatively charged hadrons in the STAR TPC and $|z| < 25$ cm constitute 80% of the total hadronic cross section[17]. Therefore, the event yield for hadronic events is given by the following equation:

$$\text{Event yield} = \text{Luminosity} \times (0.8) \times (7.2 \text{ barns}). \qquad (7.2)$$

Once the event yield is determined, by counting how many events in the data taken with the Minimum Bias trigger that have more than 7 negatively charged hadrons, the luminosity is calculated. For the data set taken with a 0.5T magnetic field strength and the Minimum Bias Trigger, the event yield for events with more than 7 negatively charged hadrons and $|z| < 25$ cm was 1,132,055 and the integrated luminosity was 196.54 $\pm$ 10% mb^{-1}. The 10% uncertainty comes from the uncertainty in the hadronic cross section.

(7.3.2) Acceptance

In order to calculate the acceptance of the detector, we used STARLight Monte-Carlo simulations. The STARLight Monte-Carlo is used to model photon-photon interactions and photon-Pomeron interactions in ultra peripheral collisions.[18] We added the X (1750) to the STARLight simulation using the mass and the width reported by the FOCUS Collaboration.[9] I assumed the X (1750) has spin 1. Since the X (1750) cannot be found in particle data books, I used values appropriate for the ϕ (1020) for constants for which there was no data to guide the choice. The input parameters that were used to run the simulation are described in Appendix (A).

We produced 79,605 X (1750) $\rightarrow K^+K^-$ events with STARLight. These events are processed by another Monte-Carlo simulation, GSTAR, maintained by STAR to simulate the interactions of produced particles with the detector. This program simulates the hits in the TPC among other things: the output is in the same form as experimental data. This data is then processed by the same reconstruction software that is used for real data (bfc.C), and tracks are reconstructed. Macros we wrote to run these codes are in Appendix (A). By comparing the number of generated events with the number of events which are reconstructed subject to the same cuts that are applied to the data, we can calculate the acceptance of the detector. However, the dE/dx calibration was not identical for the simulated data and the real data. We compensated for this by shifting the log (dE/dx) values for the simulated kaons until the kaon bands for simulated and real data coincided. For the data, the log (dE/dx) cut is chosen to be greater than 0.2. For the simulated data we required log (dE/dx) greater than -0.525. Of the 79,605 events generated, 7705 were reconstructed with the same cuts used for the data. Therefore, the

acceptance of the detector for these events = 7705 /79,605 = 0.097 ± 10%. The 10% uncertainty comes from the parameters used in STARLight simulations.

(7.3.3) Cross section for Au Au → $Au^{*}Au^{*}X \rightarrow K^{+}K^{-}$

Given these values for the luminosity and the acceptance, an upper limit for the cross section for the process Au Au → $Au^{*}Au^{*}X \rightarrow K^{+}K^{-}$ can be calculated. For a Breit-Wigner distribution, 97% of the events lie within ± width of the average. The event yield is calculated by counting events in the region from (1.75-0.122) GeV/c^2 to (1.75+0.122) GeV/c^2. We observe 4.12 coherently produced events in this mass range. Therefore, at the 90% confidence level, the maximum number of events is 8.1. The upper limit for the cross section is given by

$$\sigma(\text{ Au Au} \rightarrow Au^{*}Au^{*}X \rightarrow K^{+}K^{-}) < \frac{8.1}{0.097 * 196.54\,\text{mb}}^{-1} = 0.42 \pm 14\%\ \text{mb}.$$

CHAPTER 8

CONCLUSIONS

We studied Minimum Bias data sets from the year 2001 RHIC run with 0.25 T and 0.5 T magnetic field strengths. The 0.25 T data set was analyzed to determine an optimal set of cuts to study the reaction X (1750) $\rightarrow K^{+}K^{-}$. When the cuts were applied, neither data set showed a peak at 1.75 GeV/c^2 above the background but the statistics are very low. The integrated luminosity was calculated as 196.54 mb^{-1} for the data with the 0.5 T magnetic field strength. The STARLight Monte Carlo simulations were modified to simulate the reaction X (1750) $\rightarrow K^{+}K^{-}$. This allowed us to calculate the acceptance of the detector for this reaction. The upper limit for the cross section of Au Au $\rightarrow Au^{*}Au^{*}X \rightarrow K^{+}K^{-}$ was calculated to be 0.42 ± 14% mb.

It is clear that we need more statistics in order to study this reaction. In the next Au-Au run at RHIC much more data will be collected. It is recommended that this analysis be repeated with the inclusion of the additional data.

Cross section calculations for Φ(1680):

Cross section is the probability of a collision occurring between two particles. It is related to the nature of the colliding particles and therefore gives important information about the reaction. The cross section can be calculated by observing the event yield under given conditions of beam luminosity and branching ratios of the reaction. In this study, due to the lack of experimental data, the cross section is calculated by using the interactions that are simulated with the STARlight Monte-Carlo model.

Decay modes of Φ(1680) are shown in the table below.

	Mode	Fraction (T_i/T)
Γ_1	$K\overline{K^*}(892)+\text{c.c.}$	dominant
Γ_2	$K_s^0 K\pi$	seen
Γ_3	$K\overline{K}$	seen
Γ_4	e^+e^-	seen
Γ_5	$\omega\pi\pi$	not seen
Γ_6	$K^+K^-\pi^0$	

Table (7.1): Decay modes of Φ(1680) (http://pdg.lbl.gov)

Branching ratios of Φ(1680) are shown in table 2.

Decay mode	Relative ratio
$\Gamma(K\overline{K^*}(892)+\text{c.c.})/\Gamma(K_s^0 K\pi)$	dominant
$\Gamma(K\overline{K})/\Gamma(K\overline{K^*}(892)+\text{c.c.})$	0.07±0.01
$\Gamma(\omega\pi\pi)/\Gamma(K\overline{K^*}(892)+\text{c.c.})$	< 0.10

Table (7.2): Branching ratios of Φ(1680)

Here we study the reaction in which Φ(1680) decays into K^+K^-.

$$\Gamma(K\overline{K})/\Gamma(K\overline{K^*}) = 0.07 \quad (7.1)$$

$$\Gamma(\omega\pi\pi)/\Gamma(K\overline{K}^*) = 0.1 \quad (7.2)$$

$$\Gamma(K\overline{K}) + \Gamma(K\overline{K}^*) + \Gamma(\omega\pi\pi) = 1 \quad (7.3)$$

From equations (7.1), (7.2) and (7.3), the branching ratio for $\Gamma(K\overline{K})$ =0.0598

Event yield can be give by following formula,

Event yield = Acceptance * Cross section * Luminosity,

Where, Acceptance = (branching ratios)* (reconstructed events/generated events)

In order to determine the acceptance of the detector STARlight Monte-Carlo model was used for Φ(1680) meson.

7.3 STARlight Monte-Carlo simulations

The STARlight Monte-Carlo is used to model photon-photon interactions and photon-Pomeron interactions in ultra peripheral heavy ion collisions. STARlight consists of three input files; starlight.in, starlight.dat and jet.dat. Input parameters of the starlight.in file can be modified according to the user's needs. The file starlight.dat contains differential luminosity values and the file jet.dat contains branching ratio values for jet set. These files are re-written according to the modified parameters in starlight.in file. In order to study the reaction Φ(1680) → K^+K^-, following parameters are used in the starlight.in file.

```
79  197       // Z(number of protons), A (number of nucleons)of the colliding gold ions
108.4         // gamma for the colliding ions
1.5 -1 40     // maximum and minimum values for w (the gamma-gamma center of mass
                 energy, w = 4(E1)(E2), (a -1 tells STARlight to use the default values
                 specified in setConst.f; otherwise, specific wmin here, and the number
                 of w bins in the lookup tables
4.0 80        // maximum value for y (y is the rapidity, y = 0.5 ln(E1/E2) ) and the
```

```
                number of y-bins in the cross section calculation
3             // gg or gP switch -- A 1 here will produce 2-photon channels, a
              // 2 here will produce vector meson channels with a narrow
              //resonance, and a 3 here will produce vector meson channels with
             //a wide (Breit-Wigner) resonance.
100000   // number of events to produce
663       // channel of interest (in PDG notation) (663 for phi(1680))
345333  // random number seed
2          // The form of the output.  A 1 here generates a simple text file.
             '2' generates a text file in the gstar format
             '3' generates a PAW ntuple.
5         // This number controls the nuclear breakup
          // Note that this option only works for lead or gold; it should work at
           any energy
      1 = hard sphere nuclei (b>2R)
      2 = both nuclei break up (XnXn)
      3 = a single neutron from each nucleus (1n1n)
      4 = require that neither nucleon break up (with b>2R)
      5 = require that there be no hadronic break up
           (This is similar to option 1, but with the actual hadronic interaction
           probability)
0        // 0 = no interference (i.e. turned off), 1= interference turned on
0.5      //  when interference is turned on, this gives the %age interference 0= none
           , 1=full
0.24.   // when interference is turned on, this is the maximum pt considered
            when interference is turned on, this is the number of pt bins
```

The format of the output file starlight.out is chosen so that it can be read by GSTAR.

GSTAR is a simulation program that is used to run STAR detector simulations using

GEANT software. GSTAR reads the starlight.out file and produces .fzd files that can be

read by bfc.C , the reconstruction software. Then these .fzd files are run through

StPeCMaker; to produce histograms.

For 100,000 generated events, there are only 21 events with 2 tracks and come from a

common vertex. i.e. reconstructed events = 21

Therefore, the acceptance = (0.0598)(21/100,000) = 1.2558E(-5)

For the year 2001 RHIC run, the luminosity was 565 mb^{-1}

For 1 event, cross section = $\frac{1}{1.2558E(-5) * 565 mb^{-1}}$ = 140.94 mb

Table (7.3) shows cross sections in millibarns, for productions of vector mesons.

Meson	RHIC-Au	RHIC-I	RHIC-Si	LHC-Pb	LHC-Ca
ρ^0	590	230	8.4	5200	120
ω	59	24	0.9	490	12
ϕ	39	14	0.4	460	7.6
J/ψ	0.29	0.11	0.0036	32	0.39

Table (7.3): Cross section values of some vector mesons.

Acknowledgements

I would like to take this opportunity to thank the faculty of the Department of Physics, Creighton University for offering me a full scholarship to study at Creighton. It is with deep gratitude I acknowledge their support and encouragements, without that I would never have been able to come this far.

My special thanks go to my research advisor, Dr. Janet Seger for her immeasurable support and encouragement throughout this project. I would also like to thank my thesis committee members Dr. Robert Kennedy and Dr. Phuoc Ha for their valuable suggestions and assistance.

Thanks also go to the members of the Ultra Peripheral Collisions group at STAR; Spencer Klein, Falk Meissner, Vladimir Morozov and Pablo Yepes for their suggestions and the help in numerous ways. I would also like to thank United States Department of Energy for providing funding for this work.

Most importantly I would like to thank my family members and friends in Sri Lanka for their love and support. Even though we are thousands miles far away from each other, they are always with me whenever I need them.

Last, but not least, I would like to thank Gerard for his warm emotional support. He has given me something to believe in and brought a new meaning to my life.